

**Microfluidic-Based Synthesis of Acrylamide/Sodium Acrylate Copolymer Hydrogel
for Enhanced Properties**

by

Dizhu Tong

A thesis

presented to the University of Waterloo

in fulfillment of the

thesis requirement for the degree of

Master of Applied Science

in

Chemical Engineering

Waterloo, Ontario, Canada, 2016

© Dizhu Tong 2016

Author's Declaration

I hereby declare that I am the sole author of this thesis. This is a true copy of the thesis, including any required final revision, as accepted by my examiners.

I understand that my thesis may be made electronically available to the public.

Abstract

Hydrogels are commonly used in drug delivery¹⁻³, water treatment for heavy-metal removal⁴, tissue engineering⁵, and hygienic products, and as a plugging agent for enhanced oil recovery⁶. In recent years, a number of chemical reactions and polymerization have been developed in microfluidic devices. The products in microfluidics have a better control over size, size distribution, morphology, and chemical composition. In this work, the poly (acrylamide-co-sodium acrylate) hydrogel micro-particles with enhanced properties were synthesized in the microfluidic device.

We developed a simple experimental method (inverted-chip method) to synthesize the hydrogel micro-particles in the microfluidic device. The product micro-particles have a narrow size distribution; and their morphology is similar. The swelling property was controlled by varying the feed monomer composition and crosslinker concentration.

As a result, the hydrogel micro-particles swell faster and larger than the bulk polymer. The volume swelling ratio depends on the crosslinker concentration and the ionic content in the polymer. A lower crosslinker concentration absorbs and retains more water than a higher crosslinker concentration. The high-ionic-content polymer micro-particles have a higher swelling ratio than do those with lower ionic content.

Acknowledgements

First and foremost, I would like to thank my supervisor, Dr. Chandra Mouli R. Madhuranthakam, for giving me an opportunity to work under his guidance. His passion and professional knowledge on chemical engineering continuously teaches, inspires and encourages me throughout my graduate study. This work would not be possible without his encouragement and advice.

I also would like to thank to my co-supervisor Dr. Carolyn Ren. I sincerely appreciate all the members in Dr. Ren's research group, especially Gürkan Yeşilöz, who worked closely with me on every experiment. I really enjoyed the time that we worked together.

My special thanks to all my friends in University of Waterloo who continuously support and encourage me.

Finally, I am deeply grateful to my parents, my wife and coming baby. I love you.

Contents

List of Figures	vii
List of Tables	x
Chapter 1: Motivation and Objectives	1
1.1 Motivation	1
1.2 Objectives.....	3
Chapter 2: Background and Literature Review	4
2.1 Free-radical polymerization	4
2.2 Microfluidic Reactor for Polymerization Literature Review	8
2.2.1 Single-phase polymerization.....	9
2.2.2 Droplet emulsion polymerization	12
2.2.3 Morphology.....	26
Chapter 3: Experimental	32
3.1 Material	32
3.2 Method	33
3.2.1 Pre-polymer solution and oil-phase preparation:	33
3.2.2 Chip fabrication	34
3.2.3 Droplet generation:	39
3.2.4 Polymerization of polymer micro-particles:	41
3.3 Characterization	48

3.3.1	Droplet size and size distribution:.....	48
3.3.2	Fluorescence microscopy:.....	48
3.3.3	SEM:	48
3.3.5	FTIR:.....	48
3.3.6	Elemental analysis:	49
3.3.7	Swelling test:.....	49
Chapter 4: Discrimination of Experiment Methods.....		51
4.1	Material choice:	51
4.2	Monomer Droplet Production:	52
4.3	On-chip polymerization:	56
4.4	Off-chip photo-polymerization:	61
4.4.1	Glass slide setup:.....	61
4.4.2	Polymerization in external oil reservoir:.....	63
4.4.3	Inverted-chip method:	65
Chapter 5: Result and Discussion		66
5.1	Micro-particles size and size distribution:	66
5.2	FTIR analysis:	66
5.3	Swelling test analysis and discussion:.....	73
Chapter 6: Summary, Conclusion and Future Work.....		86
Reference:		88

List of Figures

Figure 2- 1 Single phase design to synthesis PNIPAM. [from ref. (23)]	10
Figure 2- 2 N-carboxy anhydrides synthesis in single phase MF device. [from ref. (24)].....	11
Figure 2- 3 Different types of microfluidic device for droplet generation.....	14
Figure 2- 4 Left: Terrace type setup. Right: Droplet generation mechanism. [from ref (19)]	15
Figure 2- 5 Simple T junction setup. [from ref. (29)]	17
Figure 2- 6 First simple flow focus setup. [from ref. (32)]	19
Figure 2- 7 Left: chemical reaction. Right: experiment setup. [from ref. (33)]	20
Figure 2- 8 Double Y shape flow focus. Monomer solution with different dye is injected by channel 1 and 2. Oil solution is injected by channel 3. [from ref. (15)].....	22
Figure 2- 9 Cross Flow design for TPP-chitosan micro-sphere production. [From ref.(37)].....	23
Figure 2- 10 A: Single cross junction. B: Traditional double cross junction. The surfactant is added at both cross junction. C: Delayed surfactant addition method. The surfactant is only added at second cross junction for method C. The droplet is surround by surfactant right after generation to reduce the change of coalescence. (From source ³⁸)..	24
Figure 2- 11 Coaxial MF experiment setup. [from ref. (39)]	25
Figure 2- 12 Left: a) Experiment setup with mask b) rectangular polymerized monomer c) cross section view. Right: sample Jauns particle.	26
Figure 2- 13 T junction MF producing non-spherical particles from ref (46).....	27
Figure 2- 14 Left: T junction experiment setup. Right: a) Merging method to generate Janus particle. C) Two side injection method. [from reference (47)].....	29
Figure 2- 15 Left: Experiment setup. Right: optical image of Hollow structure. [from ref. (50)]	30
Figure 3- 1 Schematic diagram of flow-focusing (top) and T-junction (bottom) microfluidic device used to synthesize polymer micro-particles.....	41

Figure 3- 2 On-chip polymerization. (a) Photo-polymerization inside the serpentine. (b) Semi-on-chip polymerization.	43
Figure 3- 3 Glass-slide polymerization. The droplets flowed freely to a glass slide and exposed to UV irradiation. .	45
Figure 3- 4 Schematic diagram oil reservoir photo-polymerization. (a) Continuous phase was FC40 and oil in the reservoir filled with hexadecane. (b) Continuous phase and oil in the reservoir was FC40.	46
Figure 3- 5 Inverted chip (T junction) method. The green tubing indicates the aqueous phase inlet.	46
Figure 3- 6 Experiment setup for inverted-chip method.....	47
Figure 4- 1 Droplet leakage. The flow direction was from top to bottom. The droplet on the top was captured just before it left T junction. When it traveled along the channel, droplet broke into small pieces, as shown in optical image. A tail followed with the large drop.	52
Figure 4- 2 Optical microscopy image of monomer droplet generation. (left) flow focus junction. (right) expended chamber.	54
Figure 4- 3 CV% measurement for droplet at microchip outlet.....	55
Figure 4- 4 CV% measurement for droplet at microchip tubing outlet. Before and after processing (left and right respectively).	56
<i>Figure 4- 5 Fluorescence microscopy image of semi-on-chip photo-polymerization.....</i>	60
Figure 4- 6 Monodispersed monomer droplets on Glass slide before polymerization	61
Figure 4- 7 Off-chip polymerization. Polymerization in external oil reservoir	62
Figure 4-8 Aggregated polymer micro-particles.....	63
Figure 4- 9 Optical microscopy image of poly-dispersed polymer micro-particles.....	64
Figure 4- 10 A string of droplet in graduate cylinder for inverted-chip method.....	65
Figure 5- 1 dried polymer micro-particle. Left: before Matlab program image processing. Right Processed image. .	66
Figure 5- 2 Hydrogel FTIR spectrum. From top to bottom: Polyacrylamide homopolymer, copolymer with 55% of sodium acrylate, copolymer with 10% of sodium acrylate, sodium polyacrylate homopolymer.	68
Figure 5- 3 rescaled spectrum of 10% and 55% NaA.	69

Figure 5- 4 Chosen band and method of calculation relative peak area. The spectrum is 55% NaA monomer concentration.	70
Figure 5- 5 (left) Magnified image for Figure 5- 4 at 1 st peak area around 2950 cm ⁻¹ . (right) Magnified image for Figure 5- 4 at 2 nd peak area around 1410 cm ⁻¹	71
Figure 5- 6 Acrylate content (F1) and relative peak area (Arel) relation for different copolymer composition.	72
Figure 5- 7 Cross-linker effect on relative peak area.	73
Figure 5- 8 crosslinking density ρx and number average molecular weight between crosslinking (Mc) plot.	77
Figure 5- 9 Crosslinking density vs. Mcat different Mn value.	78
Figure 5- 10 Theoretical swelling curves for ionic polymer network. Assuming $V_{2,r} = 1$	80
Figure 5- 11 Hydrogel micro-particles after swelling (right) Matlab program processed image (left).....	81
Figure 5- 12 Hydrogel micro-particles swelling experimental result average diameter vs. swelling time. The crosslinker concentration fixed at 0.2 w/v%.	81
Figure 5- 13 Hydrogel micro-particles swelling experimental result average swelling ratio vs. swelling time. The crosslinker concentration fixed at 0.2 w/v%.	82
Figure 5- 14 The effect of crosslinker concentration on swelling ratio.	84
Figure 5- 15 The effect of ionic content% on swelling ratio.	84

List of Tables

Table 2- 1 Free-radical polymerization mechanism.	4
Table 5- 1 FTIR experiment design table	69

Chapter 1: Motivation and Objectives

1.1 Motivation

Hydrogel is defined as a crosslinked polymeric material that can swell and retain a significant amount of water within its structure; but it cannot be soluble in water⁷. Due to its high water- absorbance capacity, higher mechanical strength, and longer service life, synthetic hydrogel has attracted more research and industrial attention than natural hydrogel during the last two decades. The major applications of hydrogel have been focused on drug delivery¹⁻³, water treatment for heavy metal removal⁴, tissue engineering⁵, hygienic products, and plugging agents for enhanced oil recovery. The materials, methods and processes conventionally used to produce hydrogel are extensively reviewed by M. Ahmed⁷. Polyacrylamide- and acrylamide-related copolymer provide the major base materials for super absorbance hydrogel.

In recent years, the polyacrylamide and polyacrylamide based micro-gel is widely used in enhanced oil recovery (EOR) for water-shut-off treatment and conformance control⁸. Conformance control is a process that improves the uniformity of a flood-fluids front both vertically and areally. The water-flooding technique, which involves injecting water underground to replace the oil, creates many “thief zones” that are highly water permeable. Non-crosslinked polyacrylamide is used to increase the viscosity of fluids injected during polymer flooding. This is an EOR technique that is used primarily for mobility control. Both water flooding and polymer flooding result in poor sweep efficiency - the percentage of original oil in place displaced from a formation by flooding fluid - in a layered system (heterogeneous system). The injected fluid tends to flow into highly permeable zones. As a result, it is difficult to achieve efficient oil displacement by conventional flooding techniques. The polymer micro-gel is used primarily for conformance control when there is a high permeability contrast⁹.

Many cases that use gel in EOR—such as bulk gel, weak gel, colloidal dispersion gel and performance gel—are reviewed by M. Abdalbaki⁹. Compared to the non-crosslinked polymer used in polymer flooding, polymer gel has better mechanical stability¹⁰, thermal stability^{8,11}, shear resistance¹¹, salinity resistance¹² and chemical resistance⁸. To achieve the conformance control, polymer micro-gel can deform and pass through pore-throats due to the pressure difference. Size, size distribution, and swelling ratio are three important characteristics of the micro-gel that is used for EOR plugging agent. The size of the polymer gel needs to match with the size of the pore-throats; otherwise the micro-gel will not enter the pore or will just pass by the pore-throats. Either consequence may result inefficient conformance control^{6,13}.

Currently, the traditional method for hydrogel micro-particles synthesis involves bulk polymerization, solution polymerization, emulsion polymerization, and micro-emulsion polymerization. All of the polymerization methods mentioned above require either complex mixing units in reactors or a significant amount of surfactant and emulsion stabilizer, which is costly. In addition to their production cost, many polymerization reactions are highly exothermic. The control of reaction temperature is critical to controlling the uniformity of polymer properties such as crosslinking density, molecular weight and copolymer composition.

The polymerization in microfluidic device (MF) is a promising method to provide better process controllability, which improves the property of hydrogel micro-particles. In recent years, the MF provides a novel approach to produce uniform monomer droplet and micro-particle. Many polymerization reactions have been performed in MFs or micro-reactors, such as free-radical polymerization of Butyl Acrylate¹⁴, N-isopropylacrylamide^{15–18} and Divinylbenzene (DVB)¹⁹. This approach allows for precise control over droplet size and reaction condition. Due to the small size of droplets, the high surface-area-to-volume ratio leads the heat and mass transfer to surrounding

environment quickly. Therefore the MF-aided method produces hydrogel micro-particles with an improved control over size, size distribution, composition, and morphology²⁰.

1.2 Objectives

The main objectives of this research are to

1. Synthesize the monodispersed spherical poly (acrylamide-co-sodium acrylate) hydrogel micro-particles with controlled compositions.
2. Develop a simple and robust experimental procedure and setup to synthesize the polymer micro-particle in the microfluidic device.
3. Evaluate the performance of different experiment procedures and setups for synthesis.
4. Study the effect of monomer composition and crosslinker density on the swelling ratio.

Chapter 2: Background and Literature Review

2.1 Free-radical polymerization

Acrylamide hydrogel is usually synthesized by free-radical polymerization, which typically involves four steps: initiation, propagation, chain transfer, and termination. The mechanism of free-radical polymerization is well-studied in the literature, and is shown in Table 2-1.

Table 2- 1 Free-radical polymerization mechanism.

Steps	Mechanism
Initiation	$I \xrightarrow{k_d} 2R_{in}^*$ $R_{in}^* + M_i \xrightarrow{k_{in}} R_1^*$
Propagation	$R_1^* + M_j \xrightarrow{k_p} R_{1+j}^*$ $R_r^* + M_j \xrightarrow{k_p} R_{r+j}^*$
Chain transfer to monomer	$R_r^* + M_1 \xrightarrow{k_m} R_1^* + P_r$
Chain transfer to solvent (S)	$R_r^* + S \xrightarrow{k_s} S^* + P_r$
Chain transfer to chain transfer agent (CTA)	$R_r^* + CTA \xrightarrow{k_{CTA}} CTA^* + P_r$
Chain transfer to impurity or inhibitor (I)	$R_r^* + I \xrightarrow{k_I} I^* + P_r$
Termination by combination	$R_i^* + R_j^* \xrightarrow{k_{tc}} P_{i+j}$
Termination by disproportionation	$R_i^* + R_j^* \xrightarrow{k_{td}} P_i + P_j$

Polymerization starts with an initiation step that involves the decomposition of initiator and the initiation of monomer to form a monomer free radical. The rate of radical production, R_i , is shown in following equation:

$$R_i = 2fk_d[I] \quad (2-1)$$

where f is the initiation efficiency (which usually ranges from 0 to 1), k_d is the initiator decomposition rate constant, and $[I]$ is the initiator concentration. According to equation 2-1, the initiation rate is proportional to the initiator efficiency and initiator concentration at fixed temperature. The next step is propagation, which increases polymer chain length. The radicals react with the monomer electron pair that are held between two carbons with a sigma bond and propagate one with others. Assuming that the rate of propagation does not depend on the chain length, it can be shown that,

$$R_p = k_p[R_r^*][M] \quad (2-2)$$

The free radicals are terminated by combination or disproportionation. The rate of termination is given by the following:

$$R_t = k_t[R_r^*]^2 \quad (2-3)$$

where k_t is the termination-rate constant and $k_t = k_{tc} + k_{td}$ where k_{tc} and k_{td} are the termination-rate constants for combination and disproportionation, respectively. Assuming steady-state, the concentration of free radical remains constant: i.e., $\frac{d[R_r^*]}{dt} = 0$, and $R_t = R_i$. Therefore, free radical concentration can be obtained as follows:

$$[R_r^*] = \left[\frac{fk_d[I]}{k_t} \right]^{\frac{1}{2}} \quad (2-4)$$

Combining equation (2-4) and equation (2-2) leads to (2-5):

$$R_p = k_p \left[\frac{fk_d[I]}{kt} \right]^{\frac{1}{2}} [M] = \frac{k_p}{k_t^{1/2}} [fk_d[I]]^{\frac{1}{2}} [M] \quad (2-5)$$

The overall rate of propagation depends on k_p , k_t , k_i : monomer and initiator concentration and initiation efficiency. The majority of monomer free radicals are consumed in the propagation step, but a few of them are consumed by small molecules such as impurities, solvents, and chain-transfer agents that can affect the molecular weight of the final polymer. The corresponding rates of chain transfer are given by equations 2-6 to 2-8:

$$R_s = k_s [R_r^*] [S] \quad (2-6)$$

$$R_{CTA} = k_{CTA} [R_r^*] [CTA] \quad (2-7)$$

$$R_I = k_I [R_r^*] [I] \quad (2-8)$$

where R_s , R_{CTA} and R_I are the rate of chain transfer to solution, chain-transfer agent and impurity respectively. k_s , k_{CTA} and k_I are the rate constants of chain transfer to solution, chain-transfer agent, and impurity, respectively. The radicals are transferred to another molecule, so the activity changes. As a result, the molecular weight is reduced.

A copolymer is formed by introducing a second monomer species in the polymerization. The mechanism is shown in equations (2-9) through (2-12):



where $R_{r,1}^*$ is the monomer free radical of length r ending with monomer 1, and $R_{r,2}^*$ represents the monomer free radical of length r ending with monomer 2. k_{pij} is the rate constant of propagation of adding monomer j to monomer free radical ending with monomer i .

The Mayo-Lewis model is commonly used for the copolymerization system, which describes the distribution of monomer in the copolymer. As mentioned above, we can write the reaction rates of two monomers as follows:

$$R_{M_1} = \frac{d[M_1]}{dt} = k_{p11}[R_{r,1}^*][M_1] + k_{p21}[R_{r,2}^*][M_1] \quad (2-13)$$

$$R_{M_2} = \frac{d[M_2]}{dt} = k_{p12}[R_{r,1}^*][M_2] + k_{p22}[R_{r,2}^*][M_2] \quad (2-14)$$

Assuming quasi-steady-state, the division of these two equations yields the Mayo-Lewis equation, which given as equation (2-15):

$$\frac{d[M_1]}{d[M_2]} = \frac{[M_1](r_1[M_1] + [M_2])}{[M_2]([M_1] + r_2[M_2])} \quad (2-15)$$

where r_1 and r_2 are the reactivity ratios of two monomers, defined as:

$$r_1 = \frac{k_{p11}}{k_{p12}} \text{ and } r_2 = \frac{k_{p22}}{k_{p21}} \quad (2-16)$$

The reactivity ratio specifically depends on the reaction conditions, such as solvent, pH, monomer species, and reaction temperature. This parameter, for most of the common monomer combinations, can be found in the polymer data/property handbook and published literature.

The monomer feed composition can be shown as follows:

$$f_1 = \frac{[M_1]}{[M_1] + [M_2]} \text{ and } f_2 = 1 - f_1 = \frac{[M_2]}{[M_1] + [M_2]} \quad (2-17)$$

where f_1 is the feed composition of monomer 1, and f_2 is the feed composition of monomer 2. Combining equation (2-17) with the Mayo-Lewis equation yields equation (2-18):

$$F_1 = \frac{r_1 f_1^2 + f_1 f_2}{r_1 f_1^2 + 2f_1 f_2 + r_2 f_2^2} \quad (2-18)$$

where F_1 is the monomer 1 instantaneous composition in the polymer mixture. In this work, the instantaneous co-monomer composition is estimated by using equation (2-18), which uses monomer feed composition and reactivity ratio.

2.2 Microfluidic Reactor for Polymerization Literature Review

Microfluidic devices have large surface-volume ratios, which enhance the mass and heat transfer compared to those achieved in conventional reactors. The polymer particles synthesised via microfluidic devices generally have an extremely narrow size distribution. Many polymerization reactions have been performed on microfluidic devices, such as free-radical polymerization of butyl acrylate, n-isopropylacrylamide and divinylbenzene (DVB)¹⁹.

Polymerization reactions in microchannels can be classified into two main categories: single-phase type and multiple-phase type. Single-phase polymerization is limited by the increase in the viscosity of the polymer during the reaction, which can often cause blockage of channels^{21,22}. Therefore, the reactant concentration and conversion is usually less than that of the conversion achieved in a batch reactor. A multiple-phase polymerization is similar to an emulsion polymerization in which a continuous phase and a dispersed phase are generated. For example, oil-in-water (O/W) or water-in-oil (W/O) emulsion. A multiple-phase-type polymerization consists of monomer droplet formation followed by polymerization of the droplet. Both steps also can be integrated onto a single chip or designed into separate chips. One type of microfluidic device produces only emulsion droplets while the further reactions take place downstream in an

external reactor. The multiple-phase method makes polymerization more complex than the single-phase method; however, it has more research applications due to ease of operation.

2.2.1 Single-phase polymerization

Single-phase polymerization is the simplest technique in microfluidics. However, a major limitation of this technique is an increase in viscosity during polymerization, which can cause clogged channels, as mentioned previously. The blockage in a single channel changes the pressure and flow rate of other inlet streams. Single-phase polymerization usually requires a mixer chamber—either an active or a passive mixer—prior to the reaction channel to obtain homogenous monomer solution. The active mixer introduces a perturbation force external to the flow, such as the small magnetic bar in Wu's work²². There are other types of active mixers, such as ultrasonic, electrokinetics, thermal, and pressure-driven mixers. However, active mixers introduce complexity to the fabrication and replication procedure, which ultimately increases production cost. Passive mixers are widely used in research because they are easily made and very efficient. The main principle of passive mixing is to increase the interfacial area of two solutions and thus increase mixing. Frequently used techniques involve the multi-lamination micromixer, the split-and-recombine mixer, and chaotic micromixers. The chaotic micromixer relies on the complex channel geometry of the microchannel, which increases chaotic advection, which in turn increases mixing.

The kinetics of polymerization of p-NIPAM on microfluidic devices has been studied by V. Dan and coworkers²³. The polymerization kinetics is monitored by an in-site FTIR device that is integrated with the microfluidic device (*Figure 2- 1*). The initiator, monomer solution, and water are injected separately at inlets I to IV. The wavy channel before merging at the T junction is for stabilizing the flow and mixing the reactants. Polymerization takes place in the serpentine channel

which constitutes reaction chamber. FTIR, temperature, and pH probes are used at P1, P2, and P3, respectively, to monitor the polymerization reaction. The reaction time is precisely controlled by the length of the serpentine channel and the inlet flow rates. The FTIR spectrum of pure reactant is measured as base-line. When the reaction starts, the band reduction on NIPAM double bond indicates the consumption of monomer. The effect of concentration of initiator, accelerator and monomer, and pH were reported. Increasing the concentration of initiator, accelerator and monomer increases the rate of polymerization. To study the viscosity effects, the maximum on-chip monomer concentration was maintained as low as 300mM, and the maximum reaction time was restricted to 6.75 seconds.

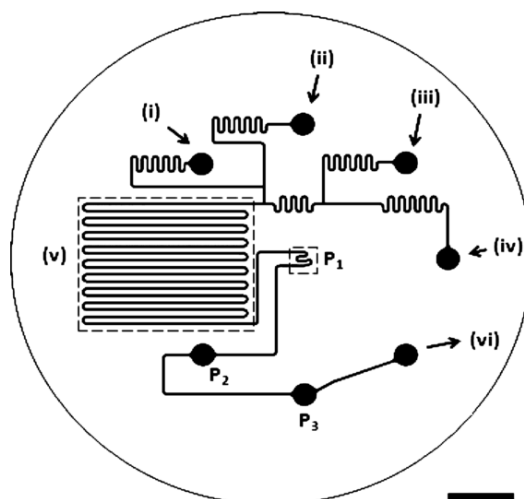


Figure 2- 1 Single phase design to synthesis PNIPAM. [from ref. (23)]

PBA, PMMA, PBMA, PS and PVBZ have been synthesized via single-phase-solution polymerization using micro-reactors by T. Iwasaki and Yoshida et al.¹⁴. The micro-reactor used in their work had mixing tubing and reactor tubing (inner diameter: 500um). To remove the heat generated by free-radical polymerization, the stainless reaction tubing was submerged under an oil bath (at 80 or 100°C). As a result, the PDI (polydispersity index, a measure of the width of

molecular weight distribution) for highly exothermic reaction in a micro-reactor is notably smaller than that of a macro-reactor.

Tao Wu et al.²² synthesized pHPMA (poly-2-hydroxypropyl methacrylate) by using a microfluidic system with an active mixing chamber, which is a small magnetic stir bar driven by magnetic stir plate. The microchannel size they used is larger than the typical size used to suppress viscosity increase during polymerization. Tao Wu et al. found that the molecular mass of polymer produced is determined by the flow rate or polymerization time. As a result, the higher the flow rate, the shorter the polymerization time; therefore, smaller conversion and molecular mass result.

Polymerization of N-carboxy anhydrides in a microfluidic device with a passive micro-mixer has been reported by T. Honda and coworkers²⁴. A schematic diagram of their microfluidic device is shown in *Figure 2- 2*. The reactor is composed of two parts: a PDMS passive micro-mixer channel and a PTFE micro-channel. The yield, molecular weight, and molecular-weight distribution of poly(amino acid) in microfluidic synthesis is compared with that in batch-wise synthesis. The molecular weight is similar, but the distribution is narrower in microfluidic synthesis, especially when the concentration of reactant is high. The mixing and temperature effects were studied. Better mixing results in a narrower MWD. Steady reaction temperature results in a smaller MWD.

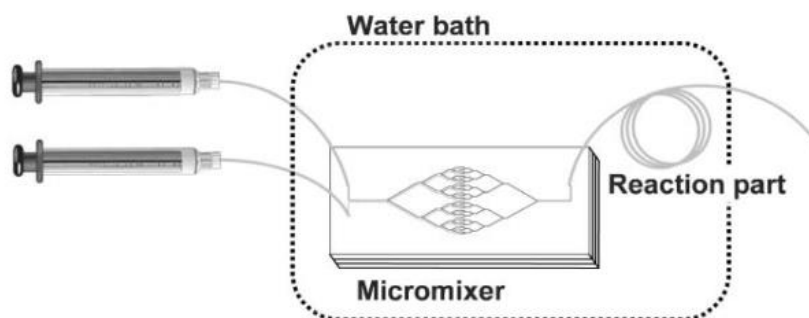


Figure 2- 2 N-carboxy anhydrides synthesis in single phase MF device. [from ref. (24)]

Enzyme-catalyzed polymerization in continuous-flow microfluidic device had been reported by S. Kundu et al.²⁵ Immobilized *Candida antarctica* Lipase B (CAL B) was stuck to aluminum micro-reactor channel wall surface by vacuum. The microchannel dimension is 2mm×1mm in width and depth, which is larger than PDMS microchannels in other reported work. ϵ -caprolactone (ϵ CL) and toluene were injected into a micro-reactor and heated the channel to a ring-opening reaction temperature (55°C to 100°C). The micro-reactor produced a faster reaction rate and larger molecular weight with the same amount of enzyme and temperature than the batch reactor. The transport path length is smaller due to the small channel dimension, and the active enzyme site is greater due to the large surface-area to-volume ratio in the micro-reactor.

A similar single-phase Styrene (Sty), butyl acrylate (BA), Sty/BA copolymer, and Methylmethacrylate (MMA) polymerization was reported by Takahide Fukuyama et al.²⁶ in a micro-flow reactor made from stainless-steel tubular reactor (length varying from 1 to 5 metres). Retention time, reaction temperature, monomer-composition effect on molecular weight, PDI, and conversion were studied. The authors report a smaller PDI, higher conversion, and higher molecular weight than those obtained with a conventional batch reactor.

2.2.2 Droplet emulsion polymerization

In recent years, polymerization in droplet has attracted more attention in research and applications²¹. Droplet emulsion polymerization generally integrates a two-step processes that includes on-chip droplet generation and post polymerization either on-chip or off-chip. There are two main categories of microsystems that can generate monodispersed droplets: microchannel-based and capillary-based devices. The common microchannel-based devices include a terrace-like microchannel device, a T-junction microchannel device, and a flow-focus (including cross-flow fusing) microchannel device. Capillary devices are typically made by inserting a tiny

capillary into glass or PDMS molding. Different microfluidic devices for droplet emulsion generation are shown in Figure 2- 3. Although there are a variety of microfluidic designs for droplet generation, the droplet size is controlled by two dimensionless numbers: Reynolds number (Re) and capillary number (Ca):

$$Re = \frac{\rho V D}{\mu} \quad (2-19)$$

$$Ca = \frac{\mu V}{\gamma} \quad (2-20)$$

where ρ and μ are the fluids density and viscosity, respectively. V is the fluid velocity and D is the characteristic dimension of the channel. γ is the interfacial tension between the two immiscible fluids. Because the flow and characteristic dimension in microfluidics is typically low, the Reynolds number is usually below unity. The capillary number represents the relative effect of viscous force versus interfacial tension force acting across an interface between the two immiscible phases. Therefore, the monomer droplet size depends on the properties of the monomer phase (such as the interfacial tension) and on the flow rates of the continuous phase and dispersed phase. In general, at a low value of Ca, larger droplets are produced. When the Ca number increases, the droplet size decreases²¹.

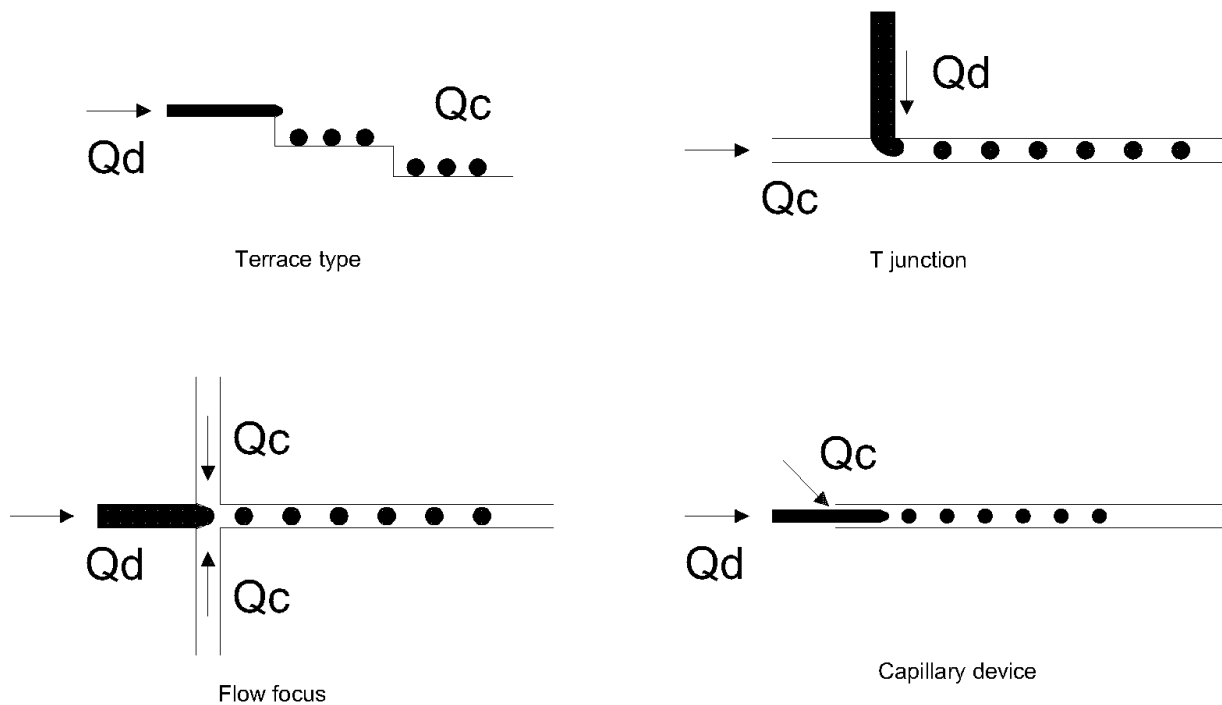


Figure 2- 3 Different types of microfluidic device for droplet generation.

2.2.2.1 Terrace type

Polymeric microsphere (MS) with narrow size distribution was synthesized by S. Sugiura et al.¹⁹ in terrace type structure microchannel (MC), as shown in figure Figure 2- 4. The channel was used for emulsion production of polydivinylbenzene. Continuous phase flows into the center channel, and the dispersed phase enters the micro-reactor on both sides of the center channel. A continuous stream of squeeze-shaped droplets form in the continuous-phase fluid when the dispersed-phase fluid passes through the microchannel. The droplets enter the terrace to form spherical droplets. The dispersed-phase solution is composed of monomer solution (DVB) and initiator solution (BPO). The continuous-phase solution is composed of surfactant (SDS) and water. The effect of

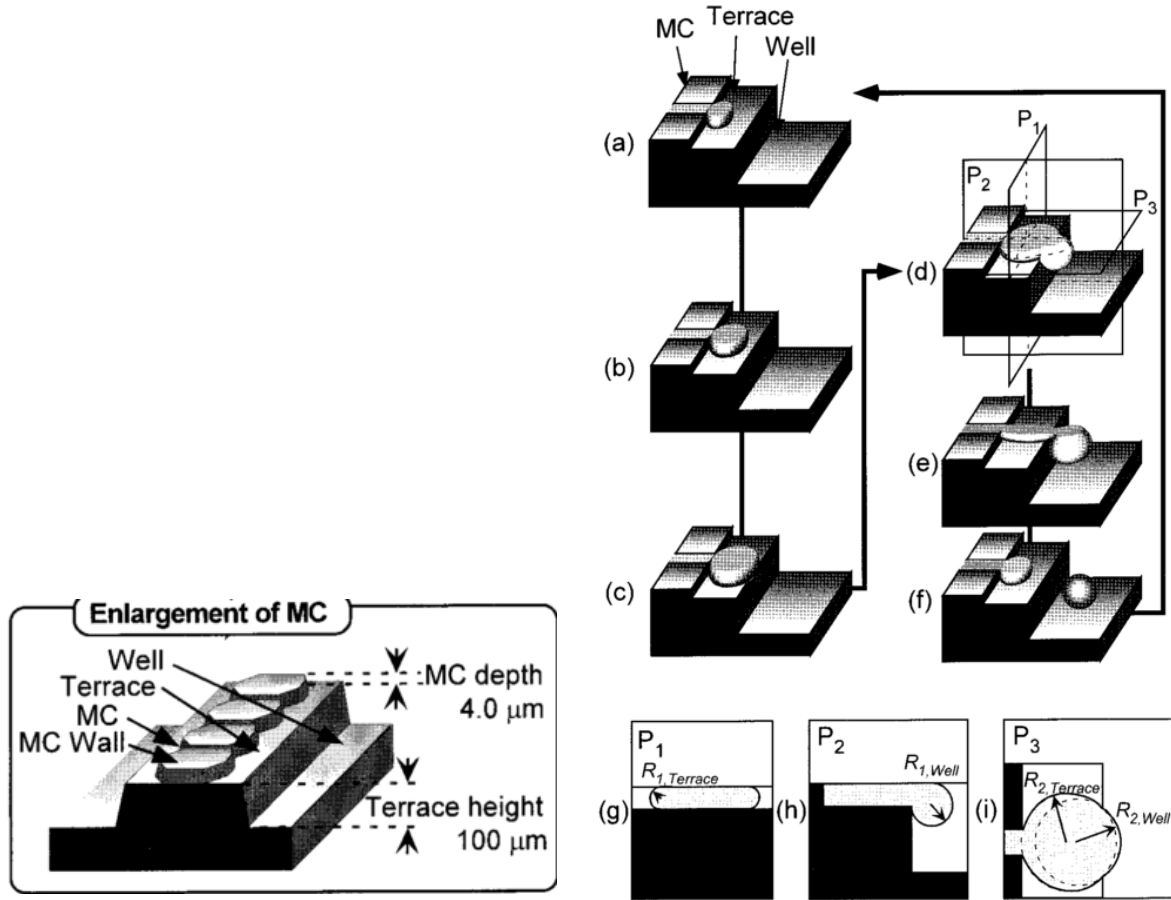


Figure 2- 4 Left: Terrace type setup. Right: Droplet generation mechanism. [from ref ⁽¹⁹⁾]

surfactant and channel width on the size distribution of polymer particles has been studied. When the concentration of surfactant is less than the critical micelles concentration (CMC, which represents the surfactant concentration above which micelles are formed), the dispersed phase forms larger droplets due to the wetting of MC. As a result, the MS has a larger coefficient of variation. The smaller MC forms smaller droplets because the MS size is smaller. However, the variation is large for smaller MC, because it is hard to control the wetting of the MC when the channel is too narrow. After polymerization, the polymer particles have a larger coefficient of variation due to Ostwald ripening.

Their first study used a simpler experiment setup²⁷. The dispersed phase is pressed into the center of a silicon microchannel plate. The continuous phase is filled in the micro channel. In this case,

they studied an oil-in-water system; therefore, the channels need to be hydrophilic after surface treatment. They studied the effect of pressure difference, which is controlled by the height of the liquid chamber, on droplet formation. The pressure required for initial droplet formation is higher than that of breakthrough. They found that the cell size is independent of the operating pressure range (1-10 kpa). The average cell size is 22.5 μm , which is 3.75 times higher than the average microchannel width.

The mechanism of droplet formation in terrace type was studied by Sugiura et al.²⁸. The dispersed phase droplet squeezes through the MC to form a flat droplet. Its size increases until it reaches the boundary of the well. The curvature of the interface increases²⁸. Consequently, the Laplace pressure, which is the pressure difference across the interface, is larger on the terrace than in the well. The change of the interface free energy before and after is calculated. As a result, $-\Delta G$ results in spontaneous droplet formation. The interfacial tension force dominates at small scales rather than other forces that influence liquid behavior. The MC system for MS formation is super-efficient with respect to energy consumption.

Ikkai F. et al.¹⁷ reported a new method for synthesizing pNIPAm gel particles that involves the use of an UV initiation system with persulfate as initiator in a terrace-type microchannel. The dispersed phase is a mixture of 700mM NIPAm monomer and 50mM APS initiator. The continuous phase is iso-octane and 5 wt% of Span 80. The maximum droplet production is 10ml/hour. Since the pNIPAm polymer and the monomer are water soluble, the MC surface was modified chemically. The droplets produced in the MC were collected in a quartz vessel for UV gelation. The average droplet size at the exit of the MC was 16 μm with a narrow size distribution. After UV gelation, there was little change in the droplet size. The gel particles absorbed water and swelled to 26.45 μm at 20°C. Due to the temperature-sensitive property of “smart gel”, it shrunk beyond critical

temperature at approximately 43°C. However, the size distribution remained below 5% during swelling and shrinking processes.

2.2.2.2 T junction

X.S. Liu et al.²⁹ synthesised poly(pentaerythritol triacrylate) (PPETA) microspheres in a simple T-junction channel design, as shown in figure *Figure 2- 5*. The microfluidic chip is made from PDMS and exhibits two perpendicular channels (diameter: 375 μm), which are the continuous- and the dispersed-phase channels. Silicon oil was pumped through the continuous phase and PPETA prepolymer was pumped through the dispersed-phase channel. The droplet formed at the junction area. After pre-polymer microspheres formed, they were collected and photo-polymerized under 365 μm UV light. PPETA monodispersed microspheres were successfully synthesised in various sizes ranging from 150 μm to 600 μm by varying the flow ratio of continuous phase and dispersed phase.

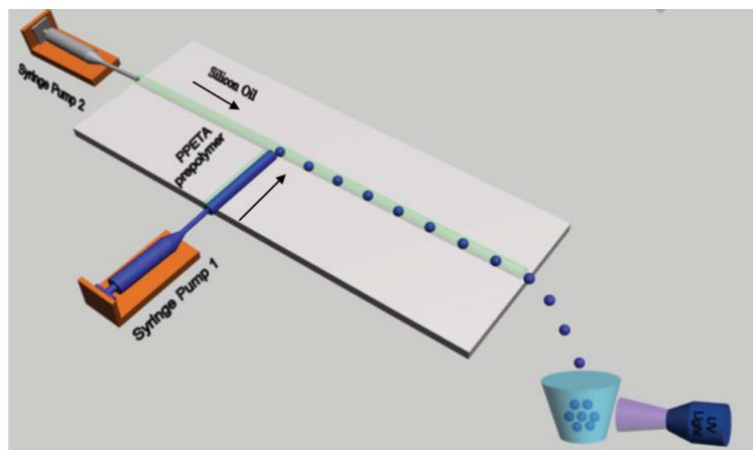


Figure 2- 5 Simple T junction setup. [from ref. (29)]

1,6-hexanediol diacrylate was successfully synthesised by photo-initiation in T-shaped channels by N. Takasi et al.³⁰. The droplet size depends on the flow rate of the continuous phase (Q_c) and the monomer phase (Q_d). For a fixed Q_d , the monomer phase wets the top surface of the channel at a low Q_c or low Reynolds-number region; once the flow reached the pocket region,

monodispersed droplets formed. As Q_c increases, the breaking point for droplet formation moves closer to the T junction. When the critical Q_c is reached, further increase in Q_c results in poly-dispersed droplet formation. Furthermore, the breakup point moves away from the T-junction point. The dicolored polymer was synthesised by thermal initiation by using a combination of Y junctions and sheath-flow junctions. Isobornyl acrylate was dyed into black and white with carbon-black and titanium-dioxide pigments. Both colors can be clearly distinguished in the droplet; however, they become less distinct after curing.

Reversed T junctions have been reported by Chia-Hsien Yeh et al.⁵ for Ca-alg micro-particle synthesis using PMMA microfluidics. The dispersed phase flows through the horizontal channel, and the continuous phase flows in the perpendicular channel. However, to the best of our knowledge, the reversed T-junction design was never used for polymer synthesis.

C.H.Choi et al.³¹ report a special T junction winding channel that uses a PDMS microfluidic device for alginate hydrogel in *in situ* production. A Y-shaped channel (for the dispersed phase) was attached to the side of the main channel (for continuous phase); therefore, the dispersed phase can have two components. Calcium chloride and sodium alginate form in the dispersed phase. The continuous phase is n-hexadecane with surfactant Span 80. The crosslinked hydrogel forms after the two components in the dispersed phase contact each other. The reaction depends on diffusion between the two components. Also, laminar flow with high retention time has the risk of coagulating. The effective of flow rate, surfactant concentration and viscosity of the dispersed phase have been studied.

2.2.2.3 Flow Focus

The first report of a flow-focusing method in a microchannel for droplet formation was introduced by Shelley et al.³² in 2002. A very simple flow-focusing geometry is implemented in the design, as shown in *Figure 2- 6*. The dispersed phase (water) flows in the center channel, and the continuous phase (oil) flows through the side channel. These liquids are forced to flow through an orifice, resulting in the formation of droplets. The droplet size depends on the size of orifice and on the flow-rate ratio of dispersed phase and continuous phase. If the droplet breaks inside the orifice, a satellite droplet accompanies the regular-sized droplet. Coalescence occurs at the outlet of the orifice if the flow rate is low; however, it can be suppressed by stabilization (adding surfactant to continuous or dispersed phase).

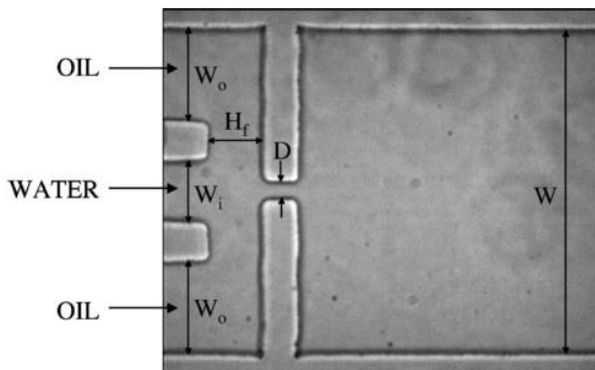


Figure 2- 6 First simple flow focus setup. [from ref. (32)]

Multi-step, microfluidic polymerization reaction was studied by W. Li et al.³³. The schematic diagram of a micro reactor is shown in *Figure 2- 7*(right). They used a passive-mixing, serpentine channel prior to the cross-flow focus junction. An interpenetrating polymer network of polyTPGDA and polyurethane was synthesized as the final product. The TPGDA is initiated by photo-initiation, and the polyurethane reaction is thermally activated by heat released from the first polymerization reaction. TPGDA and PU-pre monomers and other initiators or catalysts enter a mixer before polymerization. Droplets are formed by the flow-focusing method with polyvinyl alcohol (PVA) as continuous phase. The conversion of PU (reached 65%) depends on the heat

released by poly-TPGDA, which is easily controlled by the flow rate of TPGDA and the weight ratio of reactants consumed in reactions 1 and 2.

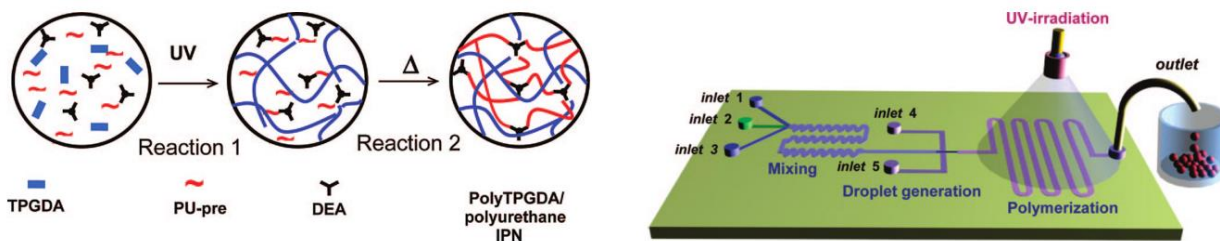


Figure 2- 7 Left: chemical reaction. Right: experiment setup. [from ref. (33)]

Adam R. et al.³⁴ suggest a novel way to generate monodisperse micro-particles from a non-Newtonian polymer solution. They report on a one-step double-emulsification method that contains three layers of solution, such as water/oil/water system. The center channel contains a non-Newtonian solution, which tends to be viscous, and is incompatible with the traditional droplet-formation technique. The middle layer and the external layer are a chaperoning fluid and a continuous-phase solution, respectively. They compared the droplet formation obtained in one-step double emulsification (novel method) and single emulsification (traditional method) for three solutions: pNIPAM, pU-pBDO, and Lipid melts. The novel method generates monodispersed polymer particles for all solutions.

A similar channel design was implemented in the copolymerization of Tripropylene glycol diacrylate- acrylic acid (TPGDA/AA) copolymer by Patrick et al.³⁵ The TPGDA/AA monomer mixture solution flows in the center channel and continuous phase flows in the outside channel. When the AA concentration reaches 10%, the droplets show a tendency to wet the channel wall, as the channel is made of Polyurethane (PU). The droplet does not break in a large range of flow rates when the AA concentration reaches 15% or higher. For the low-AA concentration case, droplet size depends on the flow-rate ratio and monomer composition. After droplet formation,

copolymer particles flow through the downstream channel for UV initiation and copolymerization. The particles are highly monodispersed.

T.D Dung et al.³⁶ report a method for the preparation of monodispersed poly(ethylene glycol) PEG micro-particles in a flow-focus MF device. Like other flow-focus MFs, the dispersed-phase (PEG) solution flows in the center channel, and the continuous-phase solution flows perpendicular to the center channel at the junction. Three flow streams force the solution into a small orifice to form hydrogel micro-particles for further UV initiation. The effect of channel geometry (different dimension of inlet, outlet and orifice), flow rate, and concentration of dispersed phase have been studied. The cured MPs are 110 to 130 μm with a CV% of 2.1%.

R.F. Shepherd et al.¹⁵ report using a Y-shaped-sheath flow-focus MF device (SFMD), as shown in *Figure 2- 8*, to generate Janus colloid-filled hydrogel granules. The MF device was made from PDMS by using soft-lithography. The dispersed phase consists of monodispersed silica microspheres in suspension in the acrylamide aqueous solution. To generate Janus granules, the colloidal suspensions are labeled by rhodamine isothiocyanate (RITC) and fluorescein isothiocyanate (FITC). Two modified suspensions are injected at two inlets of Y-shaped junctions to form a Janus laminar flow. Droplets then form in a SFMD under shearing of the sheath phase. Droplets polymerize immediately by UV initiation to retain the morphology. The optimum composition of acrylamide and silicon MPs suspension (36v/o silica and 16.5 v/o acrylamide) required to generate robust hydrogel granules is reported. The optimum concentration of

photoinitiator and acrylamide is estimated. Monodispersed spherical and discoidal colloid-filled hydrogel granules are successfully synthesised in their system.

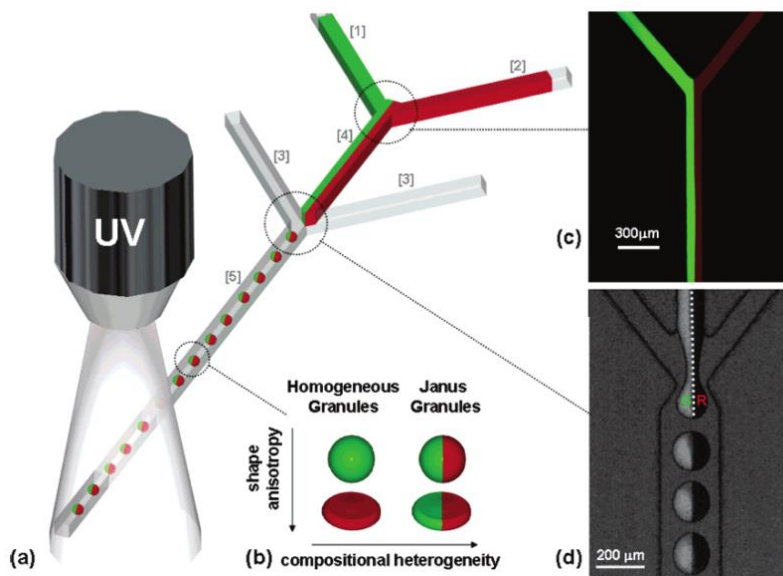


Figure 2- 8 Double Y shape flow focus. Monomer solution with different dye is injected by channel 1 and 2. Oil solution is injected by channel 3. [from ref. (15)]

2.2.2.4 Cross flow

Chih-Hui Yang et al.³⁷ introduce a cross-flow microfluidic device to generate monodispersed TPP-chitosan MS, as shown in Figure 2- 9. The microfluidic device is made of four layers of PMMA substrates. The top layer is cover layer. The second layer contains two oil inlets and a sample inlet. The third layer is the main layer, which has channels and a cross-flow junction. The bottom layer is a cover layer with three outlets. The continuous phase (sunflower seed oil) is pumped at side channels, and the dispersed phase (Chitosan sample) is pumped in the center channel. The droplets are generated when fluid passes through the crossflow junction and is transferred into a vessel with

the TPP solution for crosslinking chitosan MS by a Teflon tubing. The generated MS varies from 160 μm to 650 μm , depending on the flow-rate ratio of the two phases.

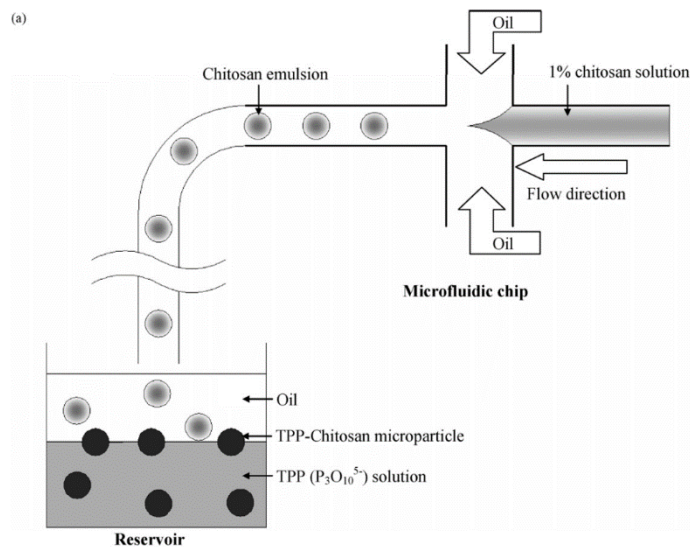


Figure 2- 9 Cross Flow design for TPP-chitosan micro-sphere production. [From ref.(³⁷)]

Droplet production in the microfluidic device is limited within the dripping regime, which is defined by capillary number (Ca) and Weber number (We). Usually, a low flow rate of inner and outer fluid is required for stable droplet generation. Seiffert et al.³⁸ introduced a delayed surfactant addition method, as shown in figure *Figure 2- 10*, to increase the droplet production from ~ 500 drops per second to ~ 3800 drops per second, which is about eight times higher than that achieved in the conventional method. For the conventional method, the flow rate for stable droplet generation is fixed at $200\mu\text{l/hr}$ for NIPAM per-microgel solution. The corresponding Ca and We numbers are 0.08 and 0.11, respectively. The delayed surfactant-addition method accelerates the flow rate up to $1600\mu\text{l/hr}$. The Ca and We numbers for the accelerated method are 0.12 and 2.02, respectively. Both methods produced monodispersed NIPAM per-polymer droplets. The per-microgel droplets are polymerized at room temperature overnight.

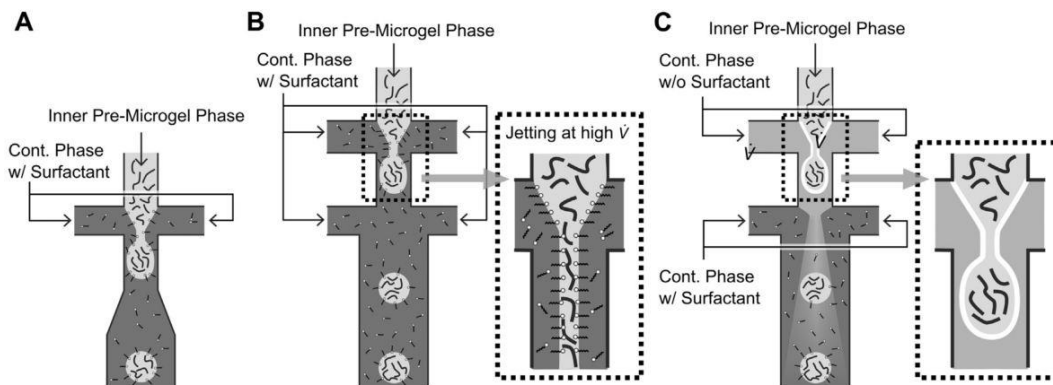


Figure 2- 10 A: Single cross junction. B: Traditional double cross junction. The surfactant is added at both cross junctions. C: Delayed-surfactant-addition method. The surfactant is added only at second cross junction for method C. The droplet is surround by surfactant right after generation to reduce the change of coalescence. (From source ³⁸)

2.2.2.5 Capillary type

The capillary type MF was often used in capsulation, microfiber, and micro-tubing synthesis. Generally, a nano-sized capillary tube was inserted in the microchannel. The dispersed phase is pumped into the center capillary tube, and the continuous phase is pumped into the microchannel. The capsulation generally combines two or more capillary devices in the co-flow or the counter-flow method. The microfiber and the micro-tubing can be synthesised in a single capillary device. As mentioned in many other review papers, the capillary type is not limited by the hydrophobicity between the MF channel wall and the dispersed phase. Therefore, the surface modification process is eliminated, which simplifies the MF fabrication.

A coaxial microfluidic device for PAM hydrogel is reported by Bodong Yang et al.³⁹, as shown in Figure 2- 11. The dispersed phase consists of acrylamide as the monomer, N,N'-methylene-bis-acrylamide as the cross-linking agent, and ammonium peroxide as the initiator. The continuous phase is n-octane. The microfluidic device is fabricated on a PMMA plate with a cylindrical Teflon capillary tube with an inner diameter of 500 μ m embedded into the plate. A Teflon microneedle (inner diameter: 160 μ m) is inserted into the capillary tube for droplet formation. The continuous

phase is injected into two side channels; meanwhile, the dispersed phase is injected into the middle channel. A PTFE tubing immersed in a heat bath which is connected to the outlet of the microchannel for the polymerization of droplets. The residence time in heat bath is approximately 1.5 minutes. After polymerization, the hydrogel micro-particles are collected in a vessel.

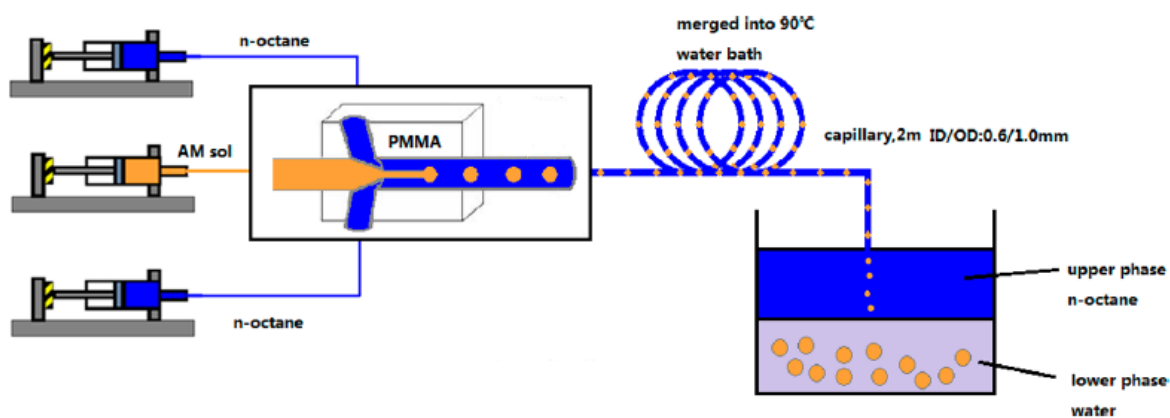


Figure 2- 11 Coaxial MF experiment setup. [from ref. (39)]

W.J Jeong et al.⁴⁰ report a sheath-flow capillary-device based on the PDMS MF device to generate MPs. This is the simplest model built on the basis of external shear force to estimate the size of droplet. The biocatalyst MPs are (glucose oxidase) immobilized on the photo-polymerizable sample.

A series of flow-focusing capillaries with a T-junction tubing system are reported by C.A. Serra et al.⁴¹. Synthesis of spherical, Janus, capsule, and rod-like microstructure polymer microbeads is successfully reported. The primary capillary is inserted to a T-junction tubing. For simple, spherical-polymer microbead synthesis, the capillary tube is connected to the second tubing for MP generation, and polymerization is done using UV initiation. For example, the synthesis of homogenous Au/PTPGDA and ZnO/PTPGDA polymer microbeads is reported by Z. Chang and coworkers⁴¹. The Janus polymer (PAM/Poly methyl acrylate for drug release study⁴² and magnetic anisotropy Janus beads⁴³) are synthesised in a side-by-side primary capillary instead of in a single

capillary. By connecting the end of first capillary to a secondary T junction tubing and a secondary capillary tail-to-head, the capsule spherical MPs are successfully generated. By adding a second layer of capillary at the end of the T-junction tubing outside of the primary capillary, the system is able to generate more beads with a controllable morphology, such as capsule and rod-like shape⁴⁴.

2.2.3 Morphology

Polymer micro-particles synthesised in the MF device can be shaped into many morphologies, which are very important in the self-assembly and other applications.

Continuous-flow polymerization can produce particles faster than multiple-phase polymerization. Dendukuri et al.⁴⁵ reports a method for synthesis of non-spherical particles in a continuous flow process using a photolithography method, as shown in *Figure 2- 12*. Polymer particles with specific shapes have been synthesised by a mask-defined UV-initiation method. Due to the permeability of oxygen in PDMS, a layer of non-polymerized oligomer acts as a lubricant layer between the channel surface and particles. The same method can also be used for the synthesis of

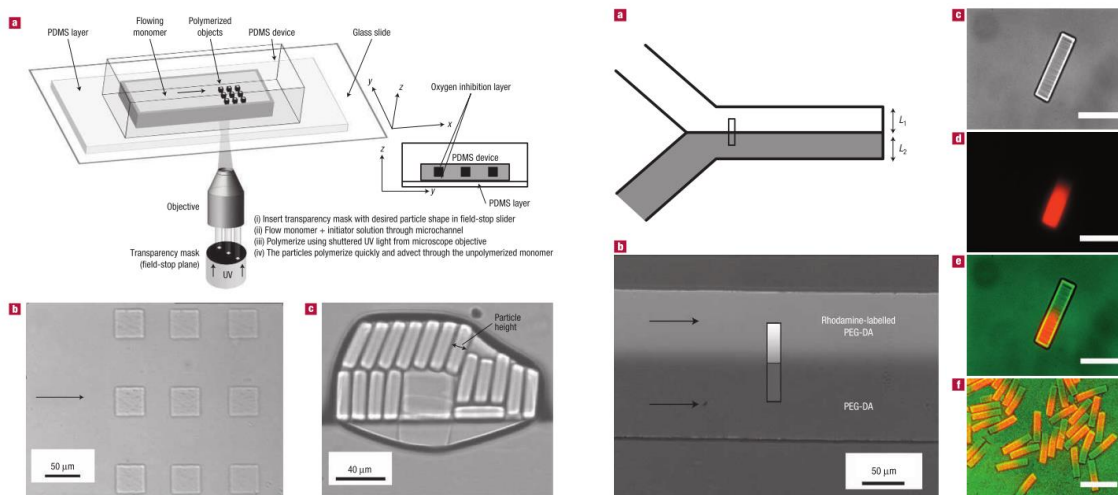


Figure 2- 12 Left: a) Experiment setup with mask b) rectangular polymerized monomer c) cross section view. Right: sample Jauns particle.

bifunctional Janus particles without premixing two reactants, which can be used in the self-assembly study.

2.2.3.1 Janus particles

Dendukuri et al.⁴⁶ reports a method to synthesize non-spherical micro-particles in microfluid by UV initiation. See *Figure 2- 13*. The droplets are formed in a T-shaped channel. The continuous phase is 1% SDS water solution, and the dispersed phase is Norland optical adhesive 60 (NOA 60), which is a UV-sensitive liquid photopolymer. According to their work, the shape of the droplet is determined by the flow rate of the dispersed phase (Q_d) and capillary. When the Ca number is too low, there is insufficient shear force for the dispersed phase to wet the top surface of the channel. When the Ca number is increased by increasing the flow rate, there is a region which forms non-spherical micro-particles. Otherwise, the particles are flat and spherical.

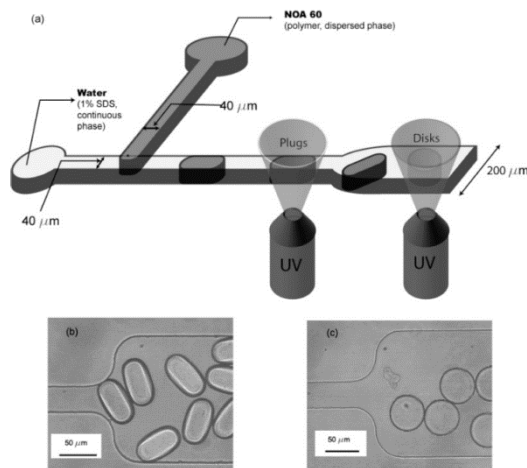


Figure 2- 13 T junction MF producing non-spherical particles from ref (⁴⁶)

Y. Bing et al.⁴⁷ studied polyethylene glycol (PEG) hydrogel in the same T-junction microfluidic with an online UV-initiation device in a rounded channel. The rounded T-junction channel is fabricated on the PDMS using the soft lithography. A rounded silica capillary is fused onto a silica

wafer by a water soluble PVA adhesive as a master framework, as shown in Figure 2- 14. The authors studied four systems: a drug-release system (mixed with Aspirin), magnetic particles synthesis (mixed with Fe_3O_4 nano-particles (NPs)), a binary PEG/dye microsphere in a peanut shape, and Janus particles. In the drug-release system, the PEG monomer is mixed with the photoinitiator 2-hydroxy-2-methyl propiophenone (HMP) and with the Aspirin, which is used as the dispersed phase. The pre-polymer microsphere is cross-linked by an online UV-initiation system. Then monodispersed MS is obtained. The size varies according to continuous/dispersed-phase flow ratio. The smaller MS releases Aspirin faster than the larger MS, as the small MS swells faster than larger one. The magnetic PEG NPs are synthesised by polymerization of PEG monomer solution and Fe_3O_4 NPs mixture. As a result, the NPs have excellent magnetic properties. In other studies, the PEG monomer solution is dyed red and blue. Peanut-shaped binary particles are formed when two solutions of different colors are pumped into different sides of the continuous phase in a staggered position. A Janus MS is formed when two colored solutions are pumped in laminar flow.

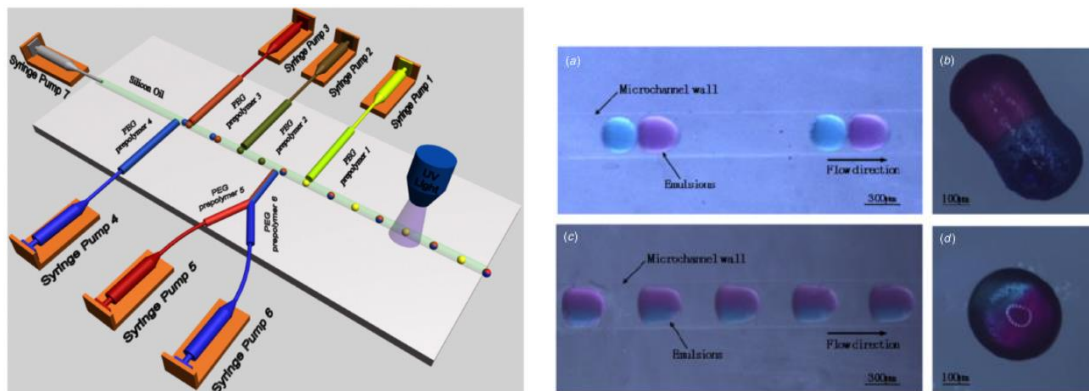


Figure 2- 14 Left: T junction experiment setup. Right: a) Merging method used to generate Janus particle. C) Two-side injection method. [from reference (⁴⁷)]

2.2.3.2 Nano-tubing:

C.H. Yeh et al.⁵ report a cross-linked Chitosan microfiber which is applied in a cell-culture preparation method in a flow-focus MF chip. The chip is made from three layers of PMMA processed by a CO₂ laser machine. The top layer has three inlets. The main channel is carved in the middle layer, and the MF is sealed by the bottom layer. Chitosan solution (injected in the center channel) is squeezed by sodium tripolyphosphate (STPP) solution (injected on both side channels) to form a laminar flow. The Chitosan is cross-linked by P₃O₅⁻ ions. The semi-crosslinked microfiber enters the STPP reservoir to complete the crosslinking. The authors studied the effect of flow rate and cell culture on the chitosan microfiber.

2.2.3.3 Hollow Micro-particles:

A novel V-junction, flow-focusing microfluidic device is introduced by Oguzhan et al.⁴⁸ to generate hollow polymer micro-particles. The device is made from polymethylmethacrylate (PMMA) by CNC machining. Three Teflon FEP capillaries (inner diameter: 150um, outer diameter: 1.6mm) are inserted into a PMMA mold, as shown in Figure 2- 15. Nitrogen gas is pumped into the center capillary. The polymer solution and the surfactant solution are pumped into two side capillaries. When the N₂ gas exits the capillary, the air bubble is surrounded by the

polymer solution immediately in the triangle area; it then releases the hollow particle to the downstream channel. The gas pressure varies between 40kPa to 350 kPa. The average particle size does not depend on the gas pressure, but the polydispersity at low pressure (40 kPa) and high pressure is much higher than moderate pressure. 20wt% of polymethylsilsesquioxane in ethanol and 18wt% glycerol and 2wt% of PVA are used to generate spherical solid nanoparticles.

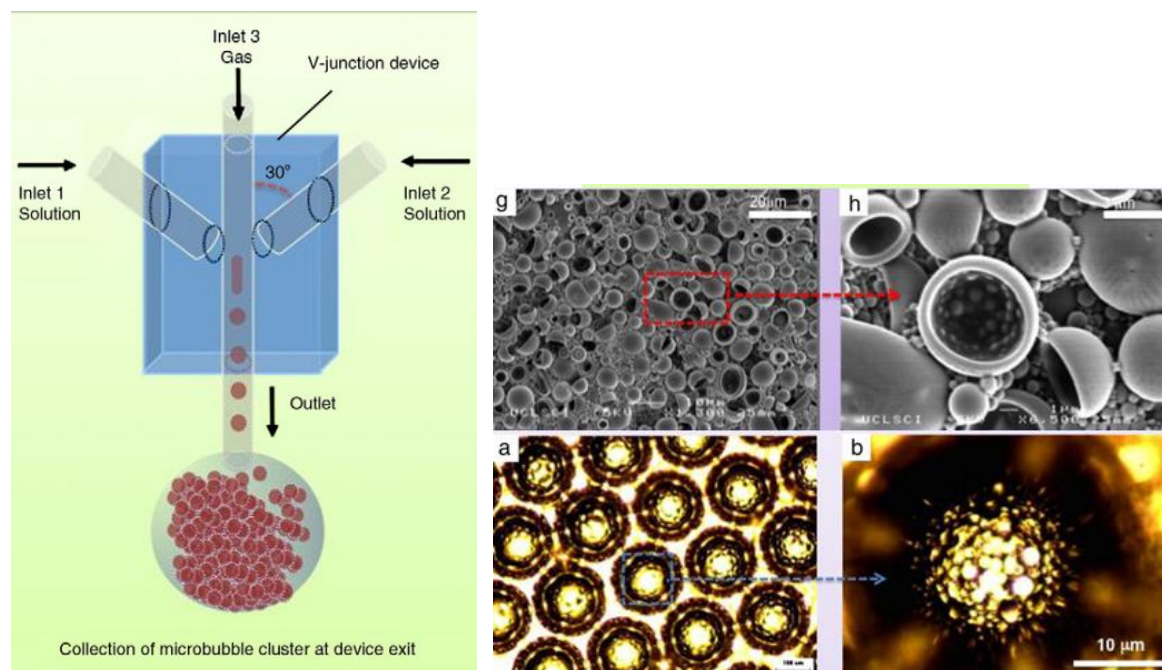


Figure 2- 15 Left: Experiment setup. Right: optical image of Hollow structure. [from ref. (48)]

A novel method of producing hollow, monodispersed, polymer micro-particles for drug-release application in microfluidics is introduced by Remigijus et al.⁴⁹ The mechanism of this method of hollow structure is based on diffusion of solvent in the dispersed phase to the continuous phase. The polymer particle continuously accumulates on the surface of the interface until a semisolid or solid surface is formed. The dispersed phase, which consists of polymer dissolved in DMC solvent, is injected into the center channel of cross-junction MF. The continuous phase, which consists of PVA dissolved in DI water, is injected into two side-channels. The flow rate is controlled within the dripping regime to minimize the polydispersity of droplet. The DMC continuously diffuses

into water, but the polymer accumulates at the interface. As a result, the droplet starts to shrink and the viscosity increases. The solvent diffusion decreases with an increase in the droplet viscosity. The controlled hollow structure performed very well in a drug-loading-and-releasing study. The encapsulation efficiency is 96-97% for this Ac-Dex polymer.

The diffusion mechanism for producing polymer micro-particles was first reported by T. Ono et al.⁵⁰ to synthesize polystyrene and poly(methyl methacrylate) micro-particles in a flow-focused MF. The effect of molecular weight, solvent, polymer concentration, and additives on micro-particles morphology have been studied.

A novel multi-stimuli responsive micro-particle for smart drug releasing application has been synthesised and reported by Jie Wei et al.¹⁸. The double emulsion chitosan micro-particle (O/W/O) is made from a double capillary microfluidic device. The smart micro-particle integrates pH, temperature, and magnetic responsive properties in one particle. The middle aqueous layer contains the pH-sensitive component chitosan, the temperature-sensitive component poly(N-isopropylacrylamide-co-acrylamide, and magnetic nanoparticles.

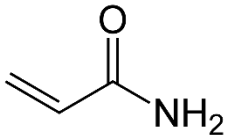
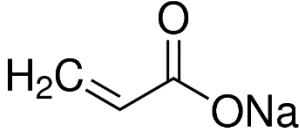
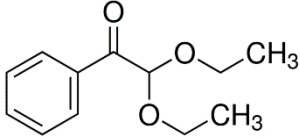
In conclusion, according to the literature review, the microfluidic device improves the properties of polymer micro-particles, yielding uniform size distribution, uniform morphology, fast swelling, and fast releasing. Multiple microfluidic designs and experimental methods exist whereby polymer micro-particles with various morphologies can be obtained. Due to the large surface-area-to-volume ratio of the droplet, the polymerization reaction can be precisely controlled in microfluidics. Therefore, we propose a novel method to synthesize the poly(acrylamide-co-sodium acrylate) micro-particles with enhanced properties in a MF.

Chapter 3: Experimental

3.1 Material

Photoresist SU-8 was purchased from Microchem Co. (MA, USA). Pre-polymer Sylgard 184 Silicon Elastomer Kit (poly-(dimethylsiloxane) (PDMS)) was purchased from Dow Corning Corp (Midland, MI, USA). Monomer acrylamide (Am) and co-monomer sodium acrylate (NaA) were purchased from Aldrich Canada and used as received. The photo-initiator 2,2-Diethoxyacetophenone (DEAP), the cross-linker N,N'-Methylene-bisacrylamide (BIS), and the activator Tetramethylethylenediamine (TEMED) were purchased from Aldrich Canada and used as received. The oil phase hexadecane and FC40 were purchased from Aldrich Canada and used after filtration. Other chemicals, such as the surfactant sorbitan monooleate (SPAN 80) and steric stabilizer polyvinyl alcohol (PVA), were purchased from Aldrich Canada and used as received.

Table 3- 1 Chemical structure of key chemicals.

Number	Chemical	Structure
1	Acrylamide	
2	Sodium Acrylate	
3	2,2-Diethoxyacetophenone	

4	N,N'-Methylene-bisacrylamide	
5	Hexadecane	
6	FC40	
7	Sorbitan monooleate	
8	Tetramethylethylenediamine	

3.2 Method

3.2.1 Pre-polymer solution and oil-phase preparation:

Monomer solution and oil solution were prepared before injection into the microchip for pre-polymer droplet generation. To prepare a 9.28M monomer solution, 10 grams of ultrapure DI water was added to a 30ml beaker and degassed with nitrogen gas for 15 minutes to remove oxygen, which can cause inhibition during free-radical polymerization. After degassing, 6.6 grams of Am

and 0.2 grams of BIS were added to the beaker and mixed for 30 minutes using a magnetic stirrer at 400 rpm. The beaker was covered with aluminum foil while mixing to prevent UV irradiation from light. 0.127ml of DEAP was added after 30 minutes of mixing and continuously mixed for another 15 minutes. For the copolymer monomer solution, sodium acrylamide was weighed and mixed according to the feed composition. The second monomer was added as Am was added. For the lower total monomer concentration, 2 mL of 9.28M concentrated monomer solution was diluted with 2 mL of degassed DI water. Then 0.04 mL of DEAP was added into diluted solution to maintain the initiator concentration.

Two different oil phases were prepared and used for droplet generation, which are FC 40 and hexadecane. To prepare the hexadecane oil phase, 5 wt.% of DEAP and 1-2 wt.% of span 80 were added to 13ml of hexadecane and mixed continuously for 25 minutes in an ultrasound mixer (Branson, model 3510). The photo-initiator in the oil phase was added to maintain the initiator concentration in the droplet; otherwise the initiator diffuses into the oil phase rapidly due to an imbalanced concentration. A similar method is used and reported by Shepherd et al.¹⁵ and Choi et al.^{16,31}. To prepare the FC40 oil phase, 1-2 wt.% of customized surfactant was mixed with FC40. Since DEAP is immiscible with FC40, it is not necessary to add DEAP. Both oil phases were filtered with 20-micrometer filter before injection to prevent clogging of the channel due to large impurity particles or dust in the air. Silicon oil and mineral oil were used occasionally for droplet generation. The preparation procedure is similar to that used for hexadecane-oil preparation.

3.2.2 Chip fabrication

Overview of fabrication procedure:

The soft-lithography⁵¹ technique is mainly composed of two techniques: master preparation and replica molding. The first technique refers to the negative photo-resist of SU8 to relief the designed

microchannel structure on a silicon wafer. The next technique is to replicate the microchannel structure by casting liquid PDMS on the prepared silicon wafer and peeling it off after it solidifies. Next, bond the PDMS molding with a glass slide to complete the microchip fabrication. The outline of the microchannel was designed in the AutoCAD® initially; then the microchannel was printed on a transparent plastic film with a resolution of 20,000 dpi. A master with the positive microchannel relief was prepared with negative photoresist of SU-8 on silicon wafers by a photolithography technique. Multiple layers of SU-8 were coated on a clean silicon wafer via spin coating, UV exposure, and thermal crosslinking. The PDMS elastomer was prepared by mixing 40 grams of silicon elastomer base with 4 grams of curing. The pre-polymer mixture was placed into a vacuum oven, and 25 psi vacuum was applied for 20 minutes to remove excess air bubbles in the PDMS elastomer mixture. The mixture was poured onto the master and cured in an oven at 80°C for 1.5 to 2 hours depending on the thickness of the replica. After curing, the replicate was carefully peeled and cut off from the master using a sharp scalpel. Holes (c.a. 2mm) for inlet and outlet were punched at the designed position before bonding. The replica and a clean glass slide were oxidized in a plasma-cleaner chamber for 50 seconds; then the replica was immediately sealed with a glass slide. Finally, Teflon tubing was attached to holes for the inlet and outlet to complete the fabrication. Microchannel wall surface treatment followed the fabrication process. In this project, water-in-oil droplets were generated. Therefore the microchannel wall surface needs to be treated hydrophobically.

Detail fabrication procedure:

The whole process begins with the designing of the microchannel with the aid of a computer program (AutoCAD®). The outline of microchannel was drawn in the AutoCAD. Then the microchannel was printed on a transparent plastic film which can be made from polystyrene or Mylar

with a resolution of 20,000 pdi. The transparency of plastic film and the printing resolution must be of good quality; otherwise, the defect on the film and channel edges can be transferred to the next step, thereby causing imperfections. The mask printing was done by Cad/Art services, Brandon OR. The finished master was stored properly in an anti-static bag to prevent dust in the air and any potential damage such as bending or scratching.

Once the mask was ready, the master was made by negative photoresist. A robust and precise master is critical for future replicate. It determines not only the precession of the microchannel but also the number of replicas that can be made from the master.

Before fabrication, SU-8 at different viscosities was prepared 24 hours before the spin-coating process. The SU-8 was poured from the shipping bottom to a smaller UV-protective container and transferred it to a pipettor. (Alternately, one could cover the container with an aluminum foil instead of using a UV-protective container.) Bubbles generated during pouring and transferring will dissolve before spin coating. The higher viscosity of SU-8 creates a higher spin-coating thickness, but it adheres less to the Si wafer; therefore, to choose the right SU-8 is critical to the master fabrication. The silicon wafer was air cleaned and baked at 200°C for 10 minutes to remove moisture on the surface (dehydration baking), as the dirt or moisture on the wafer surface prevents the SU-8 from adhering. The wafer was cooled to room temperature on a clean surface, such as petri dish.

The cleaned wafer was placed in the center of the spin chuck and aligned with the centering tool. Inappropriate alignment of the wafer can result in uneven SU-8 distribution. Once the alignment was completed, the wafer was fixed by a vacuum. To promote the adhesive of SU-8, a thin layer of low viscosity SU-8 was coated on the entire wafer. The spin coating machine was programmed in advance according to the SU-8 thickness requirement. A typical procedure is as follows:

1. 0-500 @ 100 rpm/s hold for 25s as dispensing is performed.
2. 500-SET @ 300 rpm/s and hold for 30s.

SU-8 was deposited at the center of wafer dynamically while the wafer was spinning at 500 rpm. Most of the defects in master fabrication—such as dust, air bubbles or uneven SU-8 surface—came from the spin-coating process. Therefore, this step requires much practice and attention if the product is to be protected from contamination.

After spin coating, the wafer was transferred to a hot plate for a soft bake in which the solvent was removed in SU-8 and hardened. The wafer must be in a good contact with the hot plate; otherwise, evaporation is not uniform. Smooth and steady raising or cooling is required to prevent cracking and the lift-off of SU-8. The wafer was baked on two separate hotplates at 65°C and 95°C, respectively. The baking time depends on the thickness requirement. The baked wafer was cooled at 65°C on a hotplate for 3 to 5 minutes and cooled to room temperature on a glass petri dish.

After soft baking, the wafer was exposed under UV irradiation to crosslink, and the crosslinked SU-8 was insoluble in the developer. To promote the adhesion of SU-8, a thin layer of SU-8 was coated and cured without a mask. The mask blocks UV radiation to create a positive relief on the wafer. The exposure time depends on the SU-8 thickness, UV lamp intensity and the suggested dose is given by Microchem as a reference. Insufficient exposure leads to lift-off because the crosslink does not extend to the bottom layer of SU-8. On the other hand, overexposure creates undesired features on SU-8. The wafer was put in the mask aligner and the mask was placed over the wafer. To enhance the contact of mask and wafer, a vacuum was applied (optimum pressure is 3-5 psi). Larger pressure pushes the mask into the wafer. Smaller pressure creates a gap between wafer and mask which results in an undesired shape on SU-8 after UV exposure.

The wafer required the post-bake step to complete the crosslink. The exposed wafer was baked at 65°C and 95°C on a hot plate for a few minutes (depending on the SU-8 thickness) and cooled stepwise. After this step, the channel design should be visible on the wafer.

The crosslinked SU-8 creates a positive relief on the wafer, and the uncrosslinked SU-8 needs to be removed by washing. This step is called a development process. The wafer after post baking was fixed on a dipping holder and immersed in the SU-8 developer with nitrogen bubbling for slight agitation. The excess developer and SU-8 were washed off by using isopropyl alcohol and by purging with nitrogen. If the SU-8 does not cover the whole surface area of the wafer (especially on the edge area), the empty space must be covered with glue to prevent peel-off by PDMS replica. The development process and washing completes the master fabrication. The master wafer was stored in a wafer holder in a clean room.

The next step is PDMS replica and bonding with a glass slide. The master wafer was placed in an aluminum foil bowl (customized by curling up the side of an aluminum dish). The PDMS elastomer was prepared by mixing silicon elastomer base with the curing agent at a weight of 40g and 4g respectively (10:1 ratio). The heavier PDMS elastomer will create a higher moulding. The pre-polymer mixture was placed into a vacuum oven and a 25 psi vacuum was applied for 20 minutes to remove excess air from the PDMS elastomer mixture. The mixture was then poured onto the master and cured in an oven at 80°C for 1.5 to 2 hours, depending on the thickness of the mold. After curing, the replica was carefully peeled and cut off from the master using a sharp scalpel. Holes (c.a. 2mm) for inlet and outlet were punched at designed positions before bonding. The replica and a clean glass slide were oxidized in the plasma cleaner chamber for 50 seconds, and the replica was brought to contact and immediately sealed with a glass slide. Finally, Teflon tubing was attached with holes for inlet and outlet to complete the fabrication.

Surface Modification of PDMS Microfluidic Devices:

The PDMS is naturally hydrophobic (the contact angle with water is greater than 90°). However, to obtain permanent bonding, the PDMS replica undergoes an oxygen-plasma treatment, which generates silanol groups. The presence of silanol groups modifies the PDMS surface to be hydrophilic. The wall surface needs to be hydrophobic in this project to produce water-soluble polymer droplets. A different method was used to treat the surface corresponding to the oil used as the continuous phase. For FC40, Aquapel® was injected to the microchannel for two minutes after bonding. For hexadecane, the bonded microchannel was placed on the hot plate at 125°C for 48 hours.

3.2.3 Droplet generation:

The premixed monomer solution and the oil phase were introduced into the microchannel using a pressure system or syringe pumps. If a pressure system (Fluigent MFCS8) is used, the aqueous oil phase must be stored in a small plastic vial and tightly connected with a reservoir holder. Then the pressure system was connected with a reservoir by using a soft tubing. The other end of the reservoir was connected with the inlet of the microchip. The pressure system was controlled by a software program provided by Fluigent Co. The pressure stabilized quickly. If syringe pumps (Harvard Apparatus, pump 33) are used, the syringes need to be loaded with the aqueous and the oil phases before mounting on the syringe pump. The pump provided a flow with a constant flow rate. The delivered flow rate in the microchannel correlates with the inner diameter of the syringe and the microchannel cross-section area. Therefore, the set point on the syringe pump must be calculated before injection.

If a cross-flow focus-design microchannel was used (the junction region is shown in Figure 3-1(top)), the monomer solution was injected by the center channel and the oil phase was injected

by the outer inlet. For a T junction, as shown in Figure 3- 1(bottom), the aqueous phase was delivered through a microchannel perpendicular to the main channel in which the oil phase flowed. Before connecting the reservoir with the microchip, the pressure or flow rate of the oil phase was adjusted to fill the tubing initially. When the connection tubing was fully filled with the oil, it was connected to the corresponding inlet. This process was repeated with the aqueous phase. The excess air bubbles in connection tubing can be trapped at the turning point or at the junction inside the microchannel, which can cause blockage or pressure change.

The outlet was punched at the middle of the microchannel instead of at the designed outlet area, because the designed outlet might not have uniform hydrophobicity or might be partial wetted. When droplets reached the designed outlet, they broke or split into small pieces before exiting the tubing. This may be because the chemical treatment does not reach to the corner. Instead of punching at designed outlet, the hole for the outlet was punched in the middle of the microchannel.

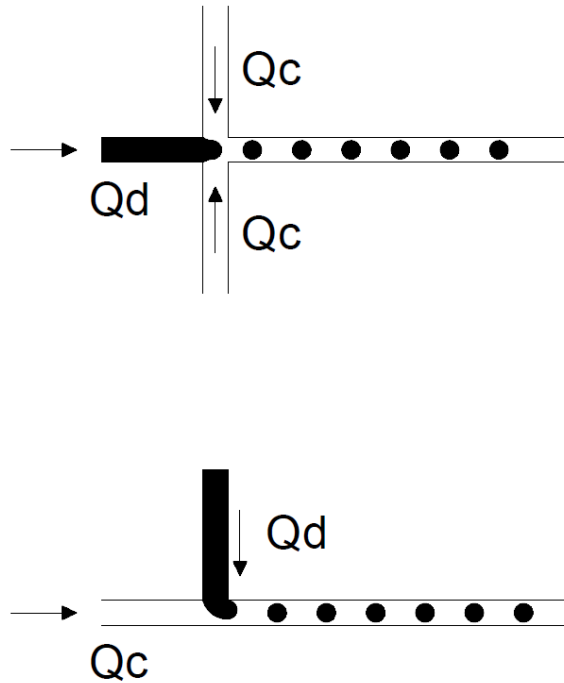


Figure 3- 1 Schematic diagram of flow-focusing (top) and T-junction (bottom) microfluidic device used to synthesize polymer micro-particles.

3.2.4 Polymerization of polymer micro-particles:

On-chip and off-chip polymerization can be used in microfluidic-aided polymer micro-particle synthesis, depending on the lab equipment and the polymer micro-particle properties required. In general, on-chip polymerization requires fast polymerization (less than 1 second) since it is limited by the dimensions of the micro-channel. To achieve fast polymerization, high initiator concentration or high UV intensity is used. However, the high initiator concentration is not economic, and it is difficult to wash out from the crosslinked polymer micro-particles. Fast polymerization may cause uninform crosslinking.

Different types of photo-polymerization of the pre-polymer droplet were carried out in this research, including on-chip and off-chip polymerization. For on-chip polymerization, droplets are

exposed to the UV irradiation immediately after droplet generation, either in a serpentine microchannel or in a PETF tube attached at the outlet (semi-on-chip), as shown in Figure 3- 2(a) and (b), respectively. Both PDMS molding and Teflon tubing have excellent UV-transmission properties. For off-chip polymerization, three methods are used: glass-slide polymerization, oil-reservoir polymerization, and the inverted-chip method (as shown in fFigure 3- 3 to Figure 3- 5, respectively).

3.2.4.1 On-chip polymerization:

The on-chip polymerization method includes polymerization in an extension wavy micro-channel (shown in Figure 3- 2a) and in an external tubing attached at the outlet (semi-on-chip polymerization, as shown in Figure 3- 2b). For the wavy channel method, n ultrahigh intensity lamp (Sunspot2, 8000W/cm² Uvitron) and a medium-high intensity lamp (ML-3500S, 50W/cm², Spectroline) were used. For the semi-on-chip polymerization, only the medium-high intensity lamp was used because the ultrahigh intensity lamp would burn the tubing after long exposure. The reaction time was controlled by the droplet-travelling time in the reaction region, which was controlled by the flow rate of the oil phase, micro-channel or tubing cross-section area, and by the length of reaction channel or tubing. Prior to UV exposure, the junction region was well covered by aluminum foil to prevent polymerization in the monomer channel. To ensure stable droplet formation, the system was stabilized for at least 10 minutes before exposure. The lamp height (measured from the top of the micro-chip surface to the lamp bulb surface) was controlled between 3 and 5 cm.

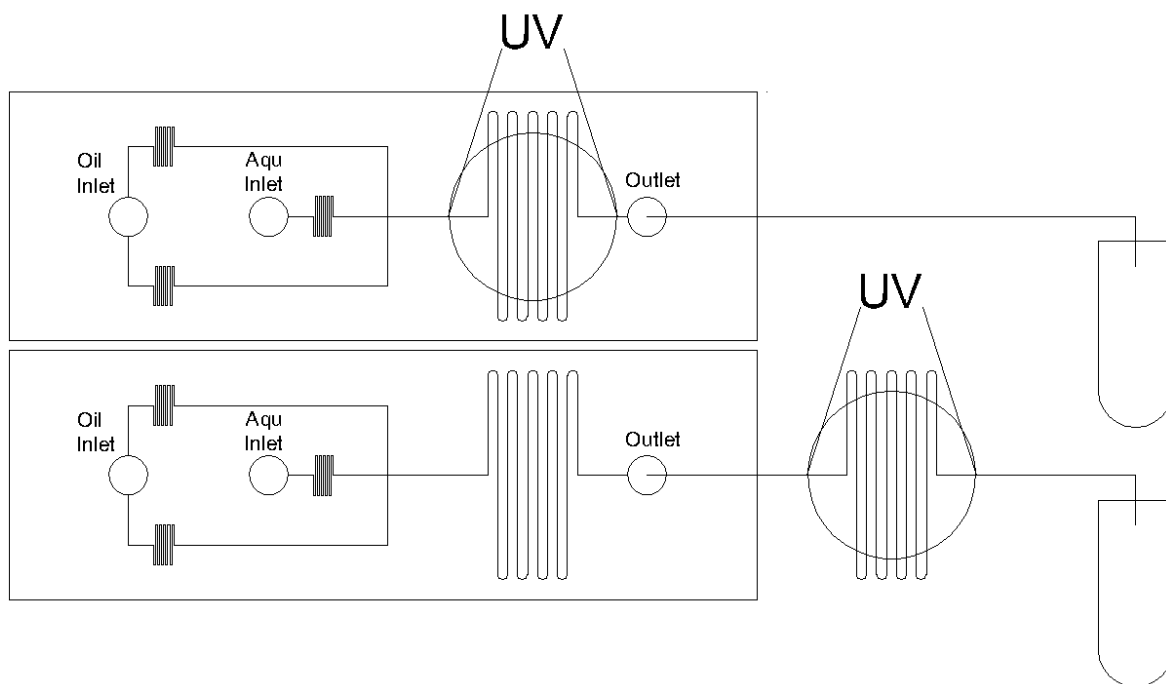


Figure 3- 2 On-chip polymerization. (a) Photo-polymerization inside the serpentine. (b) Semi-on-chip polymerization.

3.2.4.2 Off-chip polymerization:

Three off-chip polymerization methods have been studied and evaluated in this work: glass-slides polymerization, oil-reservoir polymerization and the inverted-chip method.

The glass-slides polymerization method has a different outlet, so it requires a special chip-fabrication procedure. The cured PDMS mold is cut before the designed outlet, and there is no need to punch holes for an outlet. Then the PDMS mold is bonded with a glass slide by oxygen-plasma treatment as a usual procedure. The droplet generation region is similar to that of other chips, but droplets flow directly onto the glass slide. To ensure that the droplet does not leak to the sides, a path is created by instant glue to guide the flow direction of droplets. A sketch of the microchip is shown in Figure 3- 3. The droplet accumulates on the glass side for 5 minutes and is followed by UV exposure to complete the polymerization.

For the oil-reservoir method, the droplet is collected in an oil reservoir and then exposed to UV irradiation while collecting, as shown in Figure 3- 4. Several oil-phase combinations (continuous phase and reservoir oil) were investigated, such as FC 40 in hexadecane or *vice versa*.

3.2.4.3 Inverted-chip method:

The improved oil-reservoir method is called an inverted-chip method. In the inverted-chip method, the micro-chip is flipped upside down (rotate 180°). The schematic diagram and the real experiment setup is shown in Figure 3- 5 and Figure 3- 6. The inlet and outlet holes on the PDMS molding face downward. Instead of using long, bended tubing, a short straight tubing (2 to 3 cm) is attached to the outlet and inserted into a 10 ml graduated cylinder filled with hexadecane oil phase (mixture of hexadecane DEAP and Span 80) as an oil reservoir. The cylinder is exposed to UV irradiation to collect pre-polymer droplets to complete the polymerization. The microchip is moved away from the microscope during UV exposure to prevent damage to the microscope

objective. To prevent polymerization in the monomer channel or the junction region, the whole micro-chip and the inlet tubing are covered with an aluminum foil. The junction region is carved out for observation of droplet formation. The top and bottom parts of the cylinder were covered with aluminum foil to suppress polymerization in the short tubing and aggregation at the cylinder bottom. The reaction time depends on the sinking time from cylinder top to bottom.

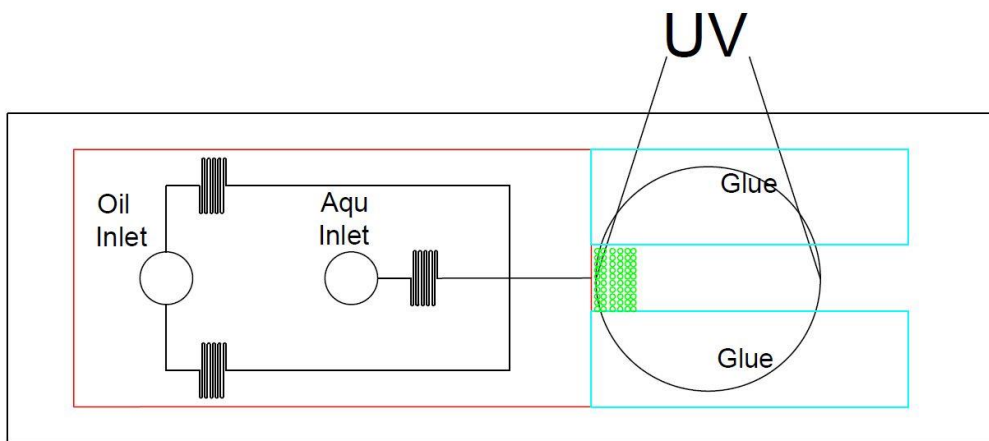


Figure 3- 3 Glass-slide polymerization. The droplets flow freely to a glass slide and are exposed to UV irradiation.

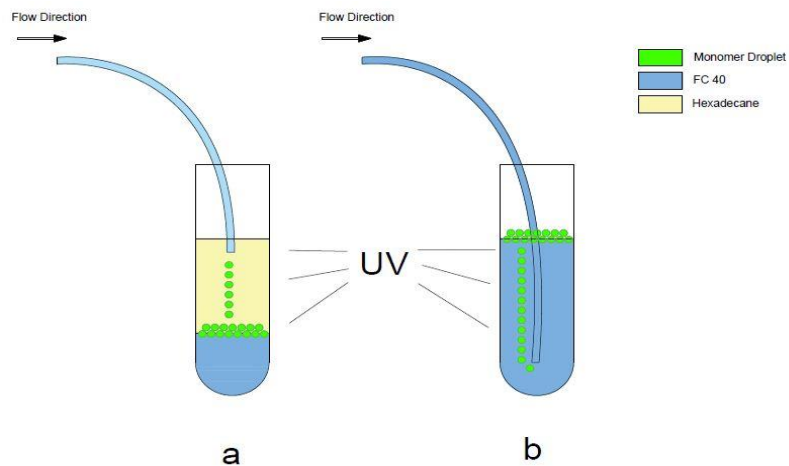


Figure 3- 4 Schematic diagram oil-reservoir photo-polymerization. (a) Continuous phase is FC40, and oil in the reservoir is filled with hexadecane. (b) Continuous phase and oil in the reservoir is FC40.

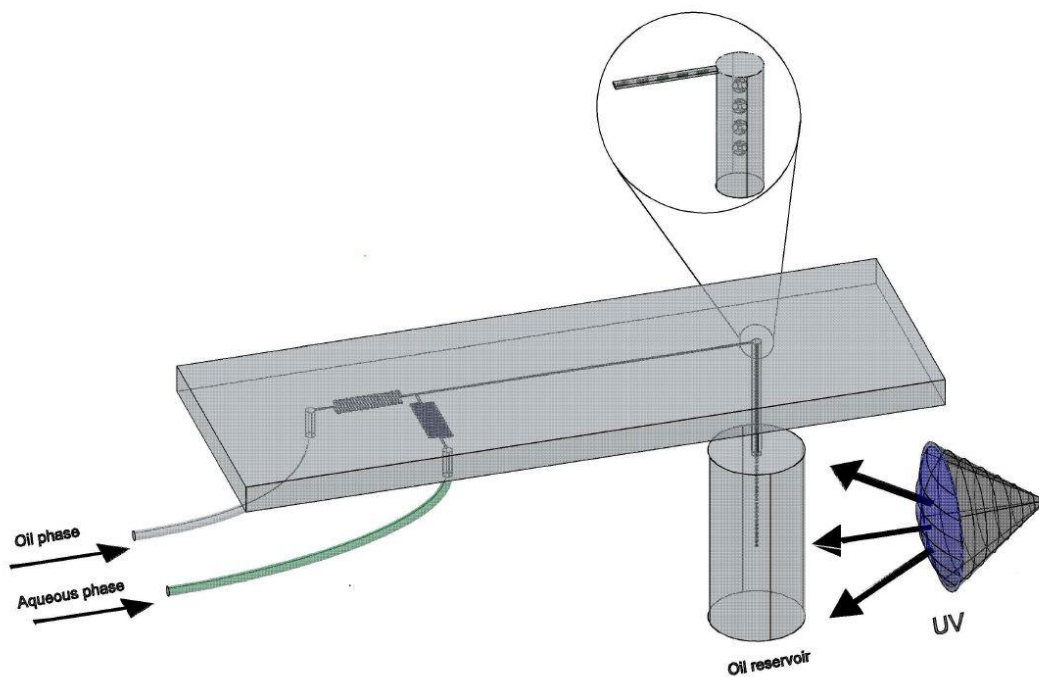


Figure 3- 5 Inverted chip (T junction) method. The green tubing indicates the aqueous phase inlet.

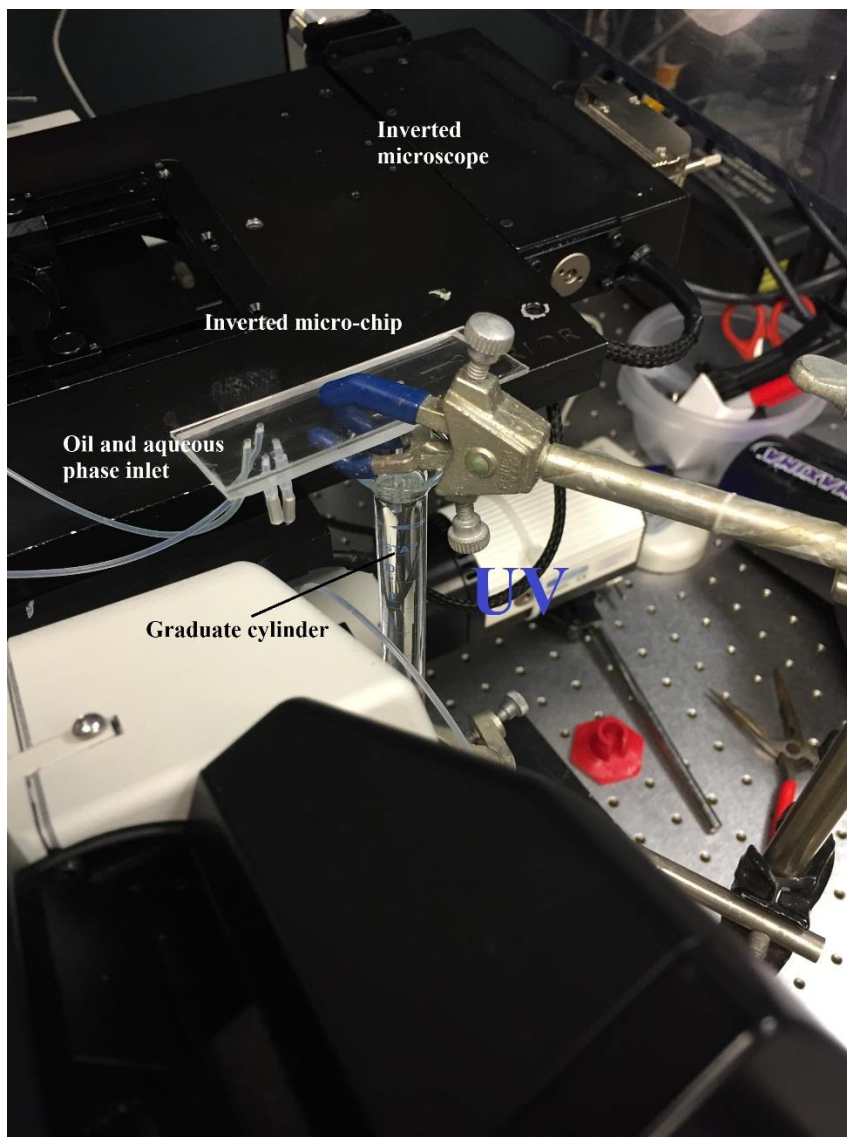


Figure 3- 6 Experiment setup for inverted-chip method.

3.2.4.4 Bulk polymer synthesis:

The bulk polymer was synthesised with the same monomer solution to compare with the polymer micro-particles. Approximately 1ml of monomer solution is added into a 10 ml beaker or a petri dish and exposed to UV light for 30 to 60 seconds until the monomer solution changes to a whitish cake. The reaction time of bulk polymer synthesis can be used to estimate the reaction time in the micro-particles experiment for the different monomer composition and concentration. The bulk polymer is washed and dried in a vacuum oven for 24 hours and stored in a desiccator.

3.3 Characterization

3.3.1 Droplet size and size distribution:

The droplet size was observed and recorded by an inverted microscope equipped with a CCD and a high-speed camera. The size and size distribution were measured and processed by ImageJ® software. The analyzed size distribution was compared with the calculated diameter variation from a MATLAB image processing program.

3.3.2 Fluorescence microscopy:

The fluorescence dye, Fluorescein (FITC) from Invitrogen, was mixed with the monomer solution before injection to the micro-channel. The fluorescence microscopy image was observed by an inverted microscope (Eclipse Ti, Nikon). The samples prepared for FTIR and elemental analysis were not mixed with Fluorescence dye to prevent contamination.

3.3.3 SEM:

Scanning electron microscopy (SEM) confirms the shape and size of dried micro-particles. Since the hydrogel micro-particle is non-conductive, a thin layer of gold is coated onto the sample surface. Images of polymer micro-particles and bulk polymers were taken at various magnifications.

3.3.5 FTIR:

The Fourier Transform infrared spectra (FTIR) of dried hydrogel micro-particles is tested by a potassium bromide (KBr) pellet method and recorded by Bruker (Vertex 70) FTIR. The scan range is from 400 to 4000 cm^{-1} for 32 times. A background scan is run every time before a sample scan.

3.3.5.1 KBr pellet method:

To prepare the KBr pellet, dry sample is crushed and ground into a fine powder, initially in a mortar. If the sample is not dry and there is leftover moisture in the polymer, the polymer is not to

be ground into a fine powder. Dry KBr granules are added into the mortar, at a weight ratio of 100:1 with respect to the polymer sample and ground into powder while mixing with polymer powder for 3 minutes. When the mixing is completed, a thin layer of white powder is spread evenly on the pellet press dies. The smooth surface of the die should always face towards the polymer powder. The pellet press die is placed under a hydraulic press at 17500 ponds pressure for 1 minute. Then the die base is removed carefully and the sample pellet is removed. A good sample should be solid and transparent. The pellet will be brittle.

If the sample pellet had a different thickness or polymer concentration, the absorbance or the transmittance of FTIR spectrum will be affected. The pellet needs to be stored in a dry condition, because of the moisture in the polymer.

3.3.6 Elemental analysis:

Polymer micro-particle composition was measured by using an elemental analysis (CHNS, Vario Micro Cube, Elementar). The blank and stand sample runs 3 times before the sample run. The content of elemental C, H, N and S in the samples was determined for calculation.

3.3.7 Swelling test:

The degree of swelling was determined by a swelling test under room temperature. The degree of crosslinking is closely related to the degree of swelling, according to the Flory-Huggins and the equilibrium swelling theories. For the micro-particle swelling test, the dried polymer micro-particles are added into a 96 well cell-culture plate, and the sizes of dried polymer micro-particles (particle diameter) are recorded by a microscope and then analyzed by ImageJ® software. The analyzed dry particle size is confirmed via SEM measurement. Then DI water, at room temperature (25°C), is added into the corresponding well. The swelling process is recorded by using a microscope. The diameter of swollen particle (at maximum absorbance capacity) is used to

calculate the degree of swelling by the following equation (assuming that the micro-particle is spherical):

$$Q = \frac{V}{V_0} = \frac{\frac{4}{3} \times \pi \times \left(\frac{D}{2}\right)^3}{\frac{4}{3} \times \pi \times \left(\frac{D_0}{2}\right)^3} = \left(\frac{D}{D_0}\right)^3 \quad (3-1)$$

where V is the volume of swollen polymer micro-particle and V_0 is the volume of dried micro-particle. D is the diameter of swollen polymer micro-particle and D_0 is the diameter of dried polymer micro-particle.

The degree of swelling of bulk polymer was measured as reference. First, 0.1g of dried bulk polymer was taken in a weight boat; it was then immersed into deionized water at room temperature for 2 to 3 days to obtain the saturated, swollen polymer. The degree of swelling is calculated via the following equation:

$$Q = \frac{\frac{(W_s - W_d)}{\rho_s}}{\frac{W_d}{\rho_d}} \quad (3-2)$$

where W_s is the weight of swollen bulk polymer and W_d is the weight of dried bulk polymer. ρ_s is the density of swollen bulk polymer, and ρ_d is the density of dried bulk polymer.

Chapter 4: Discrimination of Experiment Methods

This chapter evaluates the experiment setup, monomer and oil phase compositions, UV lamp, pumping system, and micro-chip designs.

4.1 Material choice:

Three materials were used for the oil phase in this project: hexadecane, FC 40, and silicon oil. All three materials are inert to polymerization and thermally stable. The viscosity at room temperature varies from 3mPs to 10mPs. The surfactant is mixed with the oil phase to decrease interfacial force and thereby stabilize droplet generation. Span 80 at concentration of 1wt.% to 2wt.% is used in hexadecane and silicon oil; and a customized surfactant is used for FC 40.

The photo-initiator (DEAP) is miscible with hexadecane and silicon oil. Therefore, additional photo-initiator in the oil phase maintains the DEAP concentration in the monomer solution. TEMED is an accelerator that is frequently used in the literature to trigger the redox reaction; however, the TEMED mixed in the monomer solution reduces surface tension causing droplet leakage. This phenomenon is observed only when TEMED is mixed into the monomer solution and hexadecane is used to generate droplets, as shown in Figure 4- 1. The droplet at the junction is bean shaped and remains as a whole drop. When the droplet passes certain point, a tail with tiny black droplets forms following the main droplet. The droplet leakage was observed both in the T-junction and in the cross-flow focus channel. The mechanism of droplet leakage is not clear, but reduction in surface tension could be one cause¹⁵. Another cause could be partial wetting of the channel wall surface. The monomer solution always touches the channel ceiling and floor, since the microchannel is rectangular and its height is much smaller than the channel width. If the channel surface is hydrophilic at a certain point, the droplet can break at that weak point. This

phenomenon is described in Hashimoto's work⁵² as "tip streaming" caused by a shear-driven interfacial instability exerted on the traveling droplet by the floor and ceiling.

This phenomenon is not observed when FC 40 is used as an oil phase. Therefore, FC 40 was used for the initial experimental method to avoid droplet leakage. However, FC 40 is difficult to wash with general organic solvents, such as isopropyl alcohol or acetone.

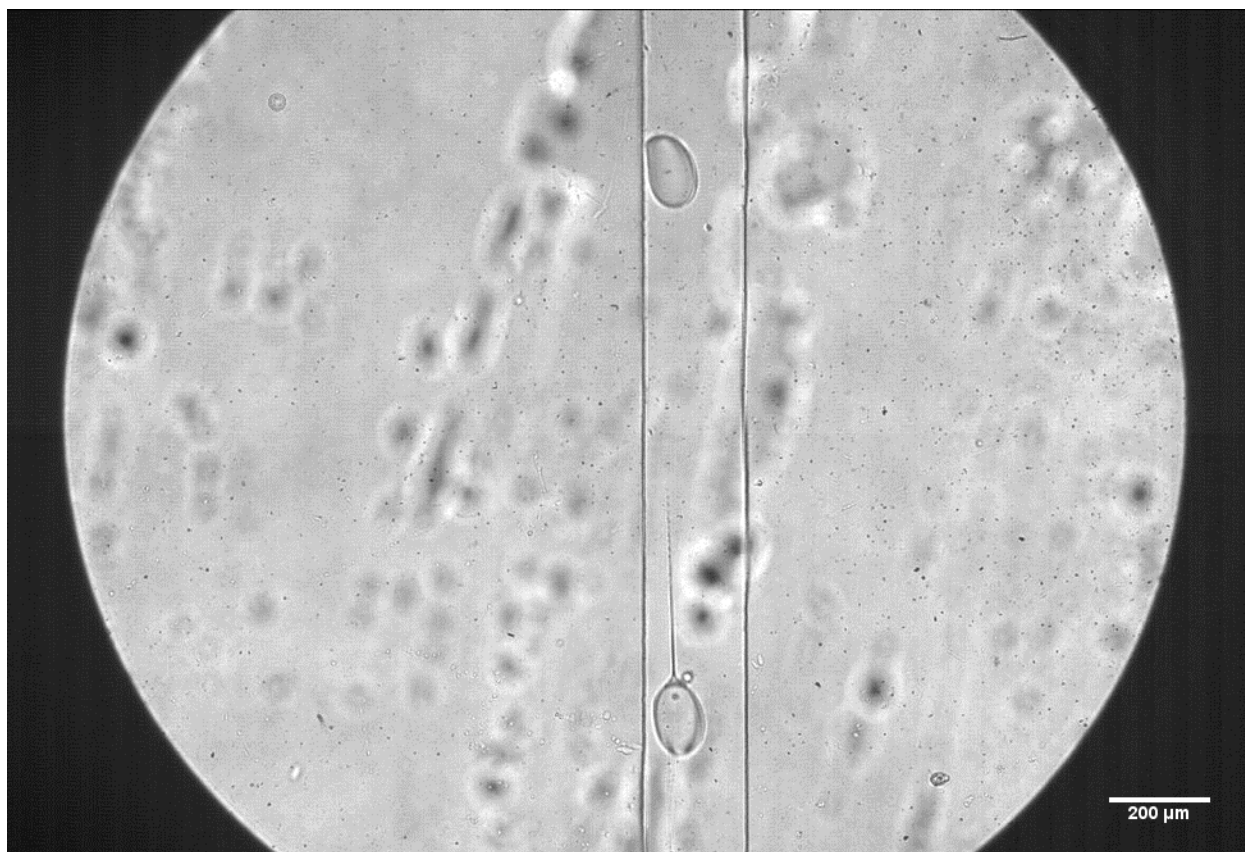


Figure 4- 1 Droplet leakage. The flow direction is from top to bottom. The droplet on the top was captured just before it left the T junction. When it traveled along the channel, the droplet broke into small pieces, as shown in optical image. A tail followed the large drop.

4.2 Monomer Droplet Production:

Monodispersed monomer droplets were successfully generated in both the T junction and the cross-flow-focus microfluidic devices, as shown in Figure 4- 1. One of the advantages of this

process is that it does not require a specific channel design for droplet generation; hence, it gives more freedom on the channel design. Droplet formation is driven by competition between viscous stress and surface tension between two immiscible fluids; therefore, the capillary number contributes to the final droplet size significantly²⁰. In addition, the droplet size is governed by the dimension of the neck region in the channel, by the flowrate ratio of continuous and dispersed phases, and by the physical properties of the two immiscible fluids. In this project, the channel height is fixed at 50 to 60 μm and the channel width at the junction is fixed at 200 micrometers. The droplet size is controlled by varying the flow rate either through syringe pumps or via the pressure system. The syringe pumps, which are commonly used in other research, provide a precisely controlled, steady flow rate inside the micro-channel, unless the channel is clogged. However, the syringe pump requires a longer time to stabilize: usually up to 30 minutes to reach steady state. Compared to syringe pumps, the pressure system responds faster to changes in the inlet pressure, and it reaches steady state quickly. Nonetheless, the pressure system suffers from a severe pressure drop in the downstream serpentine channel and external extended tubing. The pressure is sensitive to the length of the channel, to the length of extended tubing, and to the orientation of the outlet tubing (bent, vertically or horizontally oriented).

In this project, both systems are tested to match with different micro-channel designs and experimental set-ups. For example, a syringe pump is recommended for the on-chip polymerization, which requires a steady flow rate inside the microchannel to overcome the effects of viscosity change during photo-polymerization. On the other hand, the pressure system is a better choice for the inverted-chip method, as it takes less time to stabilize.

For the cross flow focus design, the center aqueous phase is symmetrically pinched off by the continuous phase at two side channels; it then broke into individual droplets of uniform size (as

shown on the left of Figure 4- 2). The droplet velocity decreases when droplets enter into an expanded chamber due to a change in velocity at the cross section area. The droplets touch each other at the chamber entrance but do not merge, which shows that the surfactant in oil phase is effective and sufficient. As mentioned above, the serpentine channel prior to the junction region, as shown in Figure 3- 2, stabilizes the inlet pressure whenever the pressure system is used. The syringe pump system provides a stable flow rate to the microchannel; therefore, the serpentine channel is not required before the junction.

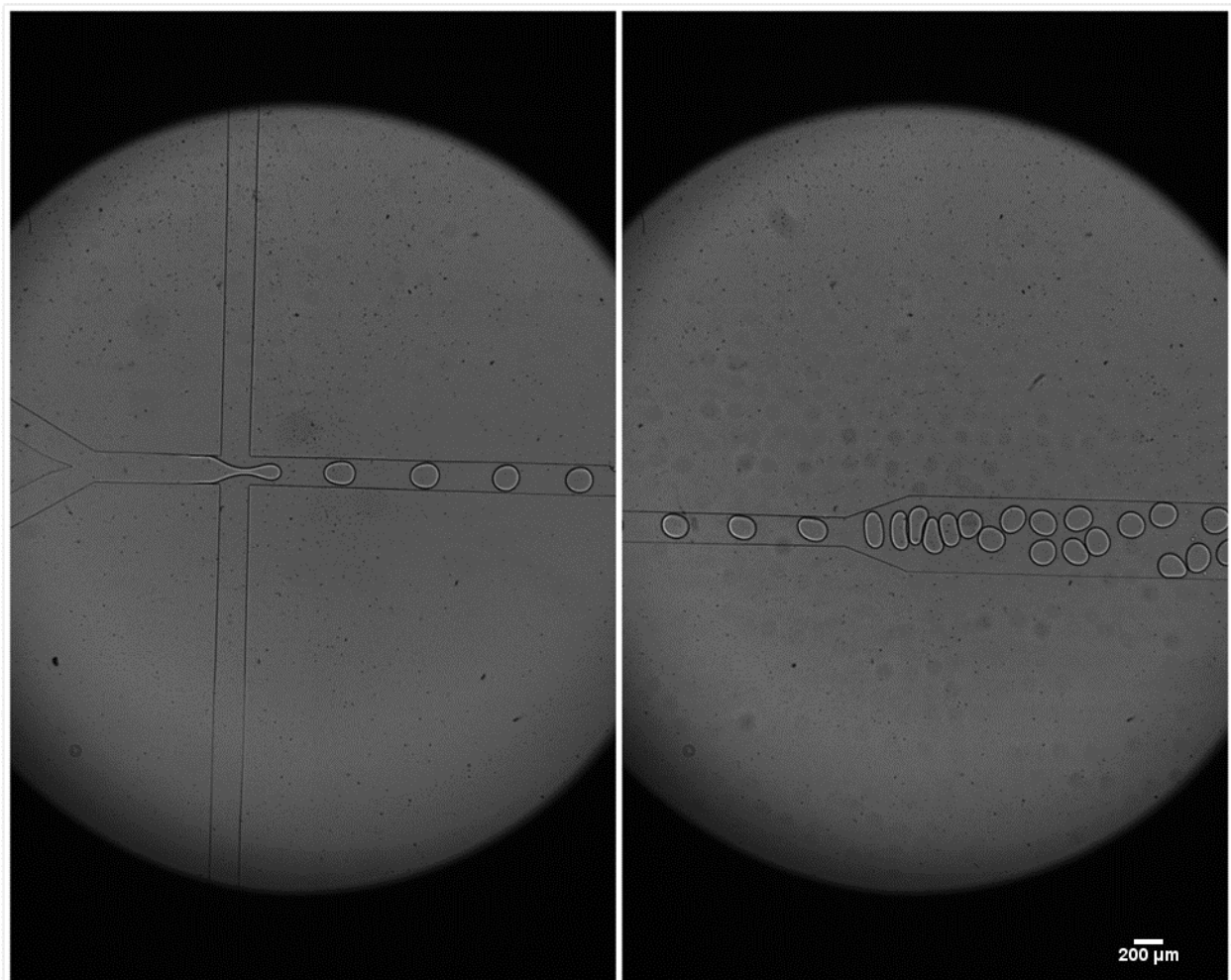


Figure 4- 2 Optical microscope image of monomer droplet generation. (left) flow focus junction. (right) expanded chamber.

Monomer droplet size is controlled by the microchannel size, by the flow rate ratio of the continuous phase, and by the dispersed phase. Since the pressure system is frequently used for fast stabilization, the inlet pressure of two immiscible phases determines the droplet size. However, due to the large pressure drop, the pressure/droplet-size relationship also depends on the serpentine channel design and the length and the inner diameter of tubing.

The droplet produced by the micro-chip has a uniform size distribution with a small coefficient of variation which is defined as the standard deviation in the measured diameter divided by the average diameter³¹. It can be calculated by using following equation:

$$CV\% = \frac{\sigma_{droplet}}{\mu_{droplet}} \quad (4-1)$$

where $\sigma_{droplet}$ is the standard deviation of droplet diameter and $\mu_{droplet}$ is the average diameter of droplets. The CV% is calculated by a MATLAB image processing program in which one can detect, capture, and measure the circular object in the image. It distinguishes the color intensity in an image automatically, such as dark or bright objective, size and void space. Figure 4-3 (left) is the original image of a droplet collected at the micro-chip outlet without any further processing. Figure 4-3 (right) is after processing. Most of the droplets are circled by red markers, including the darker ones at the bottom of the image. The droplets at the tubing outlet (inverted-chip method)

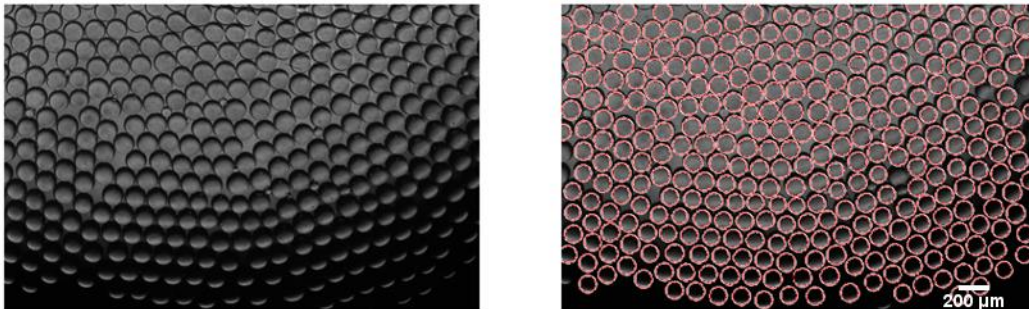


Figure 4- 3 CV% measurement for droplet at microchip outlet.

were collected on the glass slide for size-distribution analysis. As a result, the droplet has a CV% value of 3.3%, as shown in Figure 4- 4.

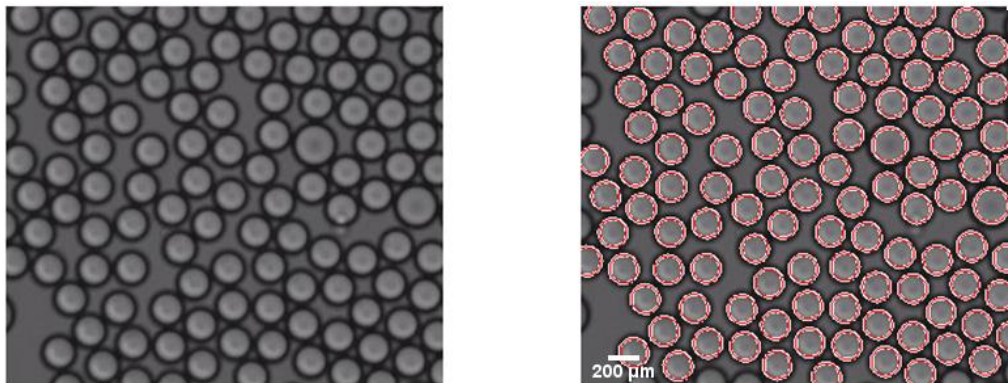


Figure 4- 4 CV% measurement for droplet at microchip tubing outlet. Before and after processing (left and right respectively).

4.3 On-chip polymerization:

The on-chip polymerization method is widely used and studied in the literature to synthesize the monodispersed, spherical, disk-like or rod-shaped polymer. Since the on-chip method polymerizes the monomer droplets individually, the product has uniform size and the morphology remains the same before and after polymerization. The on-chip reaction time (depending on the reaction-channel length and the flow rate of oil and aqueous phase) is usually less than 10 seconds. A longer reaction time requires a longer serpentine channel or a lower flow rate, neither of which are desirable for polymerization in the microfluidic device²¹. So, to facilitate the rapid reaction, one usually requires a high concentration of photo-initiator and a high-intensity UV lamp, which supplies sufficient UV irradiation that instantaneously decomposes the photo-initiator. In addition to the advanced equipment requirement, clogging (in the reaction region, the monomer supply channel, and the junction region) in the micro-channel is a serious problem that can cause wasting of the micro-chip.

An ultrahigh intensity (8000W/cm², Sunspot2 Uvitron) and a medium-high intensity (50W/cm², ML 3500S Spectroline) UV lamp were tested with the on-chip polymerization setup. With the same monomer solution, the ultrahigh intensity lamp completed the polymerization within 1 second. The reaction is fast enough that no serpentine reaction channel is required for the ultrahigh intensity lamp. The medium-high UV lamp requires 15 to 30 seconds to complete the reaction, depending on the monomer concentration. Therefore, a micro-chip with a long serpentine design was used to extend the reaction time for the medium-high intensity UV lamp.

The experimental setup with the ultrahigh-UV intensity lamp successfully produces mono-dispersed micro-particles inside the micro-channel for a short period of time (3 seconds); however, this process cannot continuously polymerize the droplets due to the microchannel clogging issue, both in the monomer supply channel and in the reaction channel. The UV irradiation focused on a spot with a diameter of 5 mm in the reaction region by a liquid-filled light guide (UVtrion). However, UV light scatters inside the PDMS mold and travels horizontally, which can initiate the monomer solution in the monomer channel and cause clogging when UV light is continuously exposed. There are different methods that can prevent the scattered light, such as blending fluoresce dye into the PDMS before curing⁵³; but all methods require a sophisticated chip-fabrication procedure. To prevent clogging in the monomer channel, we simply used two hard aluminum foils as shields inserted vertically into the PDMS mold between the reaction region and the droplet-generation junction. This simple modification blocked the majority of horizontally scattered UV light.

The other issue associated with on-chip polymerization is clogging in the reaction microchannel. This problem was observed in both UV lamp setups. The reaction in the ultrahigh UV lamp was so fast that the microchannel was clogged by aggregated polymer particles immediately after 3

seconds of operation and the clogging process could not be recorded. The decreasing velocity of partially polymerized droplets was observed and recorded in the medium-high UV lamp setup in a long, serpentine reaction channel. The inlet pressure was sensitive to the building up of pressure by the partially polymerized droplet, so the flow rate in the micro-channel changed; as a result, the droplet formation is affected. The partially polymerized droplets can be pushed away slowly by increasing the inlet flow rate in both channels. If the polymerization or gelation is completed inside the micro-channel, it will permanently clog.

Although the process of clogging is complex and the mechanism is not well understood, the potential cause and solution of micro-channel clogging is reviewed in Kumacheva's work²¹. She mentions that the aggregation of a partially polymerized droplet can lead to the clogging of a reaction channel. The drop in velocity of a pre-polymer droplet during a gelation process in the reaction region leads to the coalescence and merging of droplets into a large plug. By the time the pre-polymer droplet solidifies completely, the reaction channel is fully clogged. The recommended solution is to expand the channel size in the reaction region or reduce the droplet size. The reduction of contact between the droplets and the micro-channel wall surface minimizes the probability of clogging during the reaction. The second method is to increase the flow rate in the reaction channel to compensate the pressure drop so that the partially polymerized droplet can be pushed away.

The first recommended method was not applied in the chip design in this project. The channel height and width at the junction and reaction region was fixed at 50 and 200 micrometers, respectively. The droplet in the channel is always disk-like, as mentioned previously. If the droplet is too small, uniform size distribution is not guaranteed. In the second method, an increase in the flow rate in the reaction channel (by additional oil channel or reduction in channel width) further

reduces the reaction time and increases the contact between the droplet and the channel wall surface. Therefore, the second method did not work for the chip design in this work either.

Semi-on-chip polymerization polymerizes the droplet in the tubing to prevent clogging inside the chip. Two sizes of Teflon tubing attached to the microchip outlet were tested in this project (Inner Diameter: 750 μm and 250 μm). The droplet deformed from a disk-like shape into sphere due to the changing cross section area from rectangular to circular shape. The advantage of this method is that the droplet flows at the center in the tubing without touching the tubing wall. However, the large-diameter tubing significantly reduces the velocity of monomer droplets when they enter the tubing, so droplets can coalesce in the tubing. The tubing with a smaller diameter suppresses this problem. As a result, micro-particles synthesized in larger-diameter tubing are more poly-dispersed than they are in smaller tubing. The fluorescence microscopy image in *Figure 4- 5* shows that the product polymer micro-particles are poly-dispersed before washing. The particles in the middle are larger than the surrounding particles. The highly crosslinked polymer chain shrinks to the center; therefore, the core of droplet is darker than the shell, which indicates either a lower crosslinked density polymer or incomplete polymerization. A similar observation is reported by Bodong³⁹.

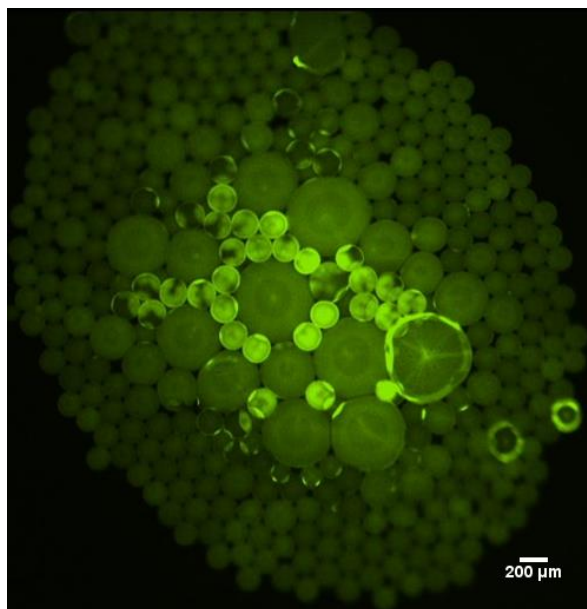


Figure 4- 5 Fluorescence microscopy image of semi-on-chip photo-polymerization.

The problem associated with this technique is that the droplet may coalesce and merge before reaction in the tubing. To enhance the observation of droplet flow in the tubing, we add fluorescence dye to the monomer solution. When the monomer droplet is exposed to UV light, it glows slightly in a dark room; so we can keep tracking the morphology and movement of the droplets in the tubing. Without the addition of fluorescent dye, the droplet is transparent in the tubing. The tubing is attached with the microchip outlet want vertically upward at the joint region initially and bend 90 degree before the reaction region. Gravity causes droplet velocity reduction in the joint region, so the droplets potentially merge. In addition, any mechanical disturbance—such as vibration or bending in tubing—will cause merging of droplets. Several variations on the tubing method were investigated, such as decreasing tubing length from 30 cm to 10 cm and reducing the bending angle; however, the coalescence in the tubing does not improve. This problem magnifies if longer tubing is used.

4.4 Off-chip photo-polymerization:

For the off-chip polymerization technique, monomer droplets are collected in a reservoir or a petri dish and exposed to UV irradiation to polymerize. This method avoids the clogging issue; however, it suffers from serious aggregation during polymerization. A similar observation is reported by Wei Li et al.³³ For the glass-slide and the oil-reservoir experiment, the monodispersed monomer droplet produces a thin film or cluster of poly-dispersed polymer micro-particles after polymerization. The inverted-chip method, developed based on the oil-reservoir method, produces monodispersed spherical polymer micro-particles.

4.4.1 Glass slide setup:

The uniform-sized monomer droplets are collected on a glass for this experimental setup. The droplets touch each other. FC 40 is the oil used for this experiment setup. It has a higher density

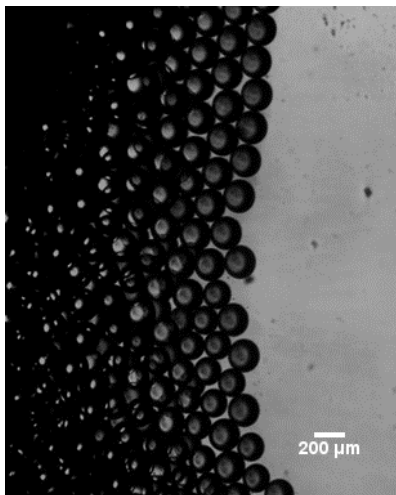


Figure 4- 6 Monodispersed monomer droplets on Glass slide before polymerization

than the monomer solution; therefore, the droplet floats on the top of oil. There are multiple vertical layers of monomer droplets close to the outlet region, as shown on the right side of Figure 4- 6.

Droplets attract each other due to interfacial force, so they do not flow directly to the end of the glass slide (flow from left to right in Figure 4- 6). The velocity decreases dramatically at the outlet exit region, so some droplets are pushed to the top layer. After exposure to UV irradiation, monomer droplets disappear, and a thin and transparent polymer film forms on the top of the oil which can be easily broken by a tweezer. The monomer droplets on the glass slide contact each

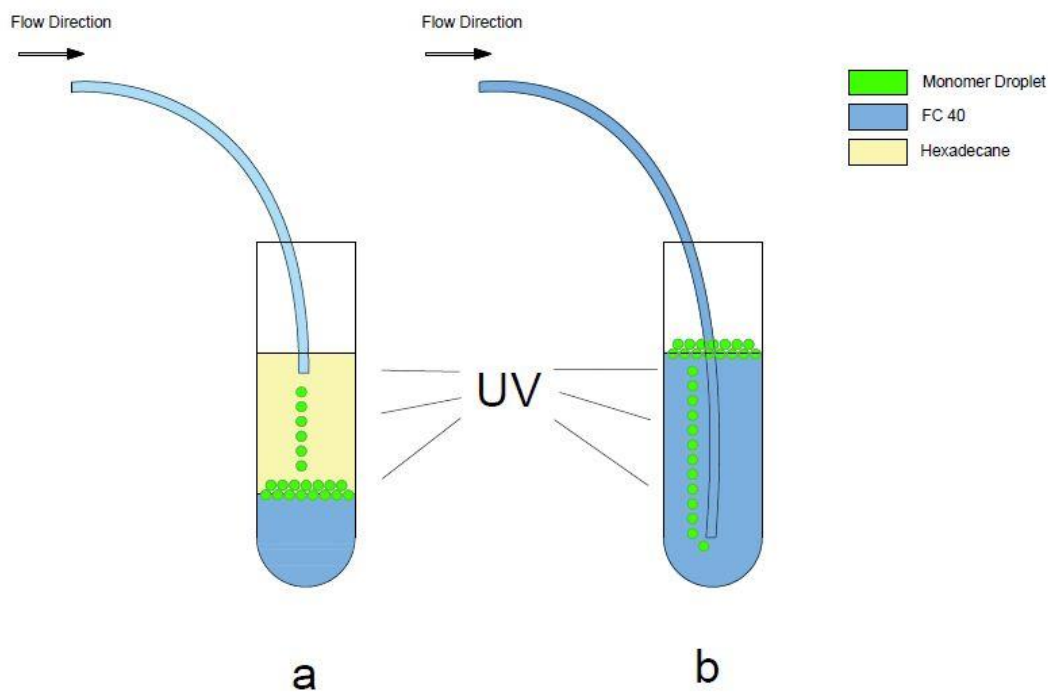


Figure 4- 7 Off-chip polymerization. Polymerization in external oil reservoir

other tightly, so they crosslink on the interface during polymerization. Therefore, the space between monomer droplets during polymerization is critical to retain the original morphology.

4.4.2 Polymerization in external oil reservoir:

The alternative off-chip polymerization method is to collect the monomer droplets in a plastic vial filled with oil, which is called an oil reservoir and is followed by UV irradiation (as shown in Figure 4- 7). The initial experimental setup, TEMED, is added to the monomer solution for faster reaction, and the FC 40 is used for the oil phase to avoid droplet leakage. The reservoir is filled with hexadecane and DEAP mixture, Figure 4- 7(a). When the outlet tubing is attached to the reservoir vial, the FC 40 sunk to the bottom and the monomer droplet floated in the middle layer due the density ($\rho_{FC40} > \rho_{monomer} > \rho_{hexadecane}$). Since these three fluids are immiscible, the FC 40 forms a large droplet (monomer droplet on top and FC 40 on the bottom) before it sinks to the bottom. Droplets sink individually and accumulate at the bottom of the reservoir. The

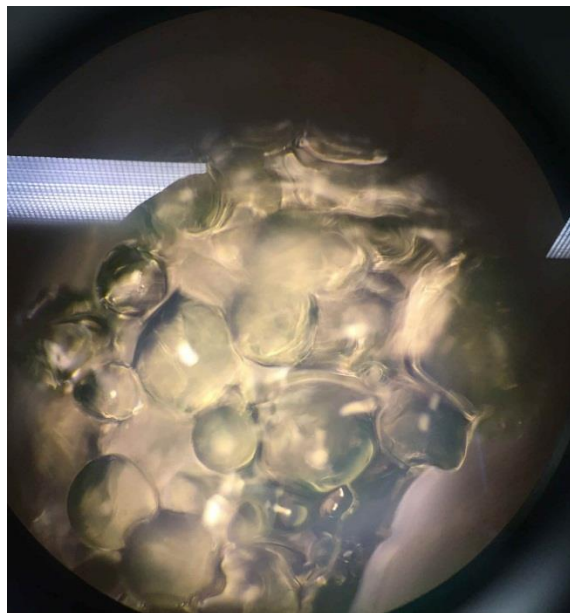


Figure 4-8 Aggregated polymer micro-particles

accumulated droplets are continuously exposed to UV irradiation. During photo-polymerization,

the partially polymerized micro-particles aggregate to form a cluster of micro-particles, as shown in Figure 4-8.

Changing the oil in the reservoir to FC40 suppresses aggregation, as shown in Figure 4- 7(b) right; but it cannot be avoided completely. In this situation, the monomer droplet floats directly to the top of oil. Therefore, the reaction time for individual monomer droplets increases. As a result, the conversion is higher and there is a smaller chance to aggregate.

To conclude off-chip polymerization, to achieve individual polymer micro-particles, the monomer droplets need to be polymerized individually and separately. Otherwise, the monomer droplets aggregate during polymerization. To increase the space, the monomer droplet is poured into a petri dish and then polymerized. However, the mechanical disturbance during pouring causes merging of small droplets to larger droplets; even so, many droplets remain individual. After polymerization in the petri dish, polydispersed polymer micro-particles are collected and washed (as shown in Figure 4- 9).

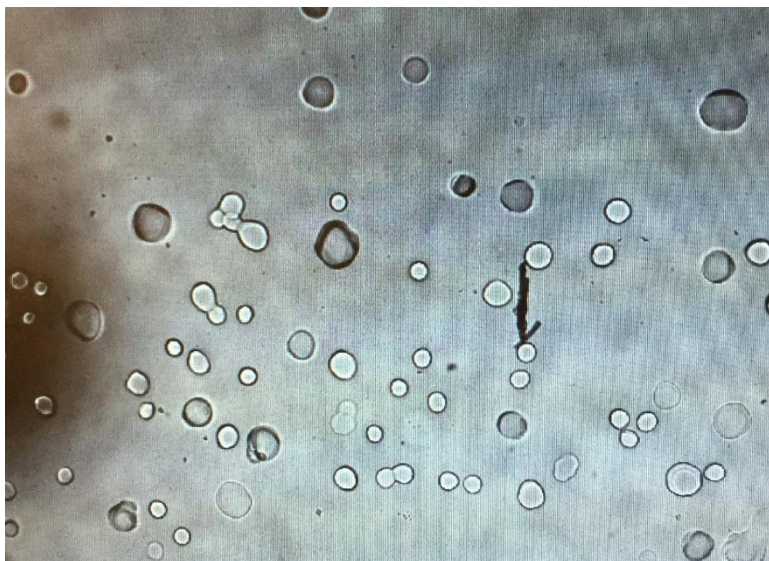


Figure 4- 9 Optical microscopy image of poly-dispersed polymer micro-particles.

4.4.3 Inverted-chip method:

The inverted-chip method is the improved version of the oil-reservoir method, which gives more uniform spherical micro-particles without the clogging issue. By simply flipping the chip 180° and attaching a short straight tubing to the outlet, droplet coalescence in the tubing is avoided. The flipped chip does not affect droplet generation, which was mentioned in the previous section. The droplet generation can be observed in the carved window at the junction region. A string of monomer droplets fell directly to the middle of the graduated cylinder without merging and coalescing, as shown in Figure 4- 10. The space between the droplets is larger than that in the on-chip method or the semi-on-chip method, so the droplets can be polymerized separately and individually. The reaction time is extended to approximately 30 seconds since the graduated cylinder is much longer than a plastic vial. The reaction time can be further extended by increasing cylinder length.



Figure 4- 10 A string of droplets in a graduated cylinder for the inverted-chip method.

Chapter 5: Result and Discussion

The mono-dispersed polymer micro-particle was successfully synthesized using inverted-chip method. Size and size distribution, composition, and crosslinking density are analyzed and discussed in this chapter.

5.1 Micro-particles size and size distribution:

After polymerization, the monomer droplet was washed with isopropyl alcohol or methanol and dried in a vacuum oven for 24 hours. It is then stored in a vacuum desiccator. The dried micro-particles are shrunk and deformed, as shown in Figure 5- 1. The dried micro-particle has a larger CV% (5.68%) than that of monomer droplets before polymerization.

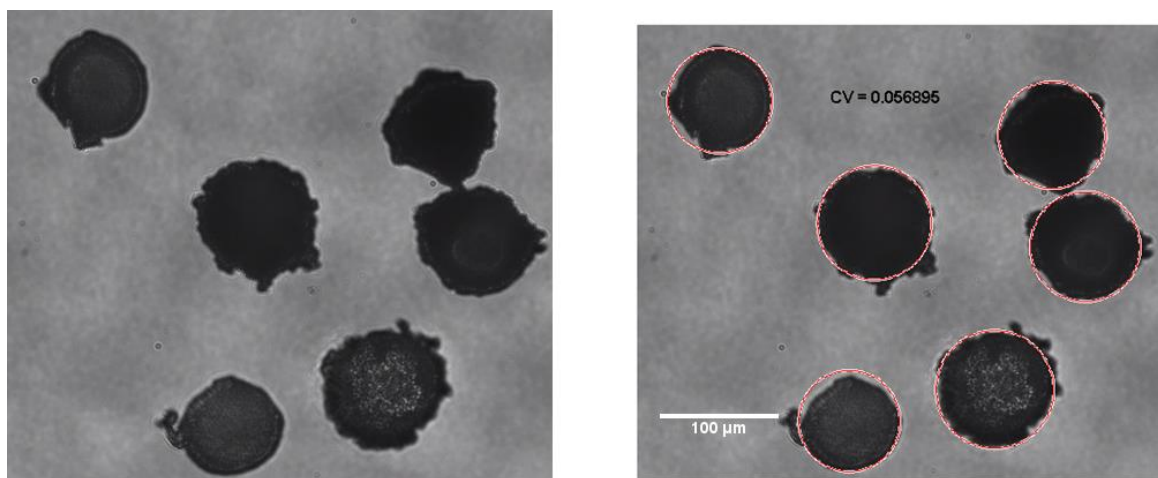


Figure 5- 1 dried polymer micro-particle. Left: before Matlab program image processing. Right Processed image.

5.2 FTIR analysis:

Experiment design:

Homo-polymer polyacrylamide and sodium polyacrylate micro-particles were synthesized and measured for reference. Then crosslinked copolymer micro-particles of acrylamide and sodium acrylate with 10% of NaA and 55% NaA are synthesized and measured. The micro-particles with different cross-linker concentrations are also synthesized and measured. The experiment design table is shown in Table 5- 1.

Table 5- 1 FTIR experiment design table

Run #	1	2	3	4	5	6
NaA% (%)	0	10	10	55	55	100
Bis (g)	0.2	0.2	0.1	0.2	0.1	0.2

Result:

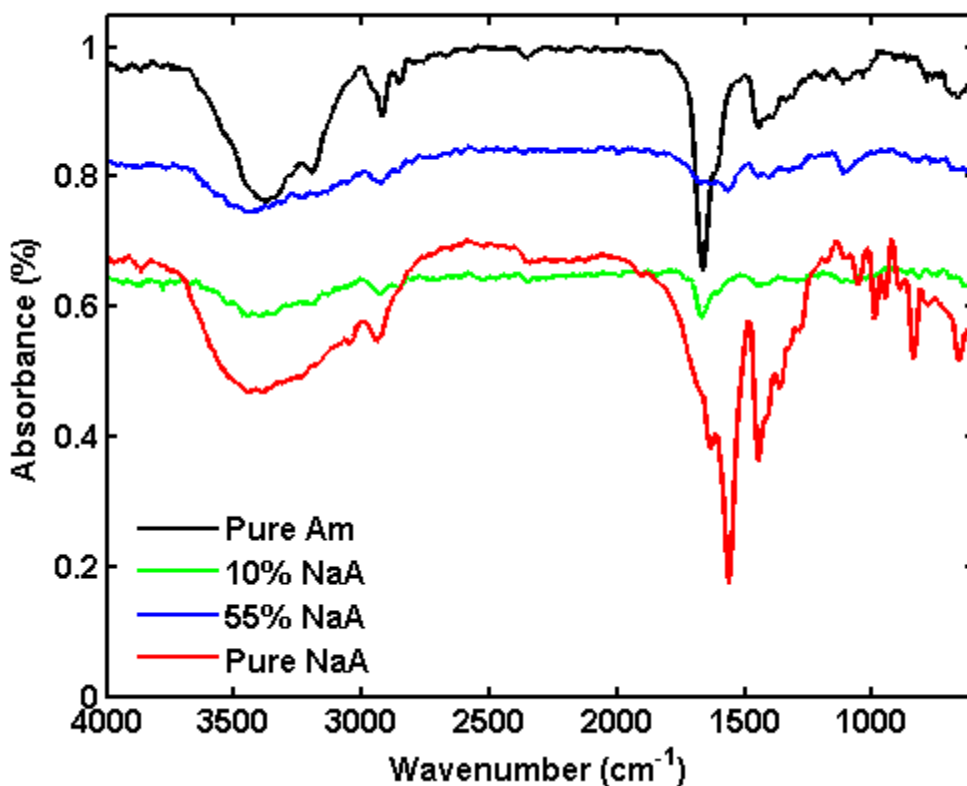


Figure 5- 2 Hydrogel FTIR spectrum. From top to bottom: Polyacrylamide homopolymer, copolymer with 55% of sodium acrylate, copolymer with 10% of sodium acrylate, sodium polyacrylate homopolymer.

According to the spectrum in Figure 5- 2, bands at $3410\text{-}3421\text{cm}^{-1}$ and $3190\text{-}3914\text{cm}^{-1}$ represent asymmetry and symmetry vibrations of the NH_2 group, which are characteristic of the acrylamide unit. Those two peaks are broadened by O-H stretch at 3300 cm^{-1} . The strong peak at $1650\text{-}1680\text{ cm}^{-1}$ indicates the C=O bond. Bands at 1560 and 1410 cm^{-1} indicate the carboxylate group stretching of COO^- group. The band at 2950 cm^{-1} is assigned to CH and CH_2 stretching. The carboxylate group at 1410 cm^{-1} is chosen as a standard to compare with different NaA compositions. The increasing peak area in bands 1410 and 1560 cm^{-1} means an increasing acrylate composition in the copolymer. From Figure 5- 2, it is difficult to distinguish the difference of absolute peak area at 1410 cm^{-1} because of the absorbance variation.

The absorbance of copolymer micro-particles is smaller than the absorbance of homopolymer that results in a lower copolymer concentration in the KBr pellet. To avoid the absorbance difference and pellet thickness difference, a relative absorbance is calculated for comparison. The relative peak was chosen at CH and CH₂ stretching at 2950 cm⁻¹, which is shown in every spectrum.

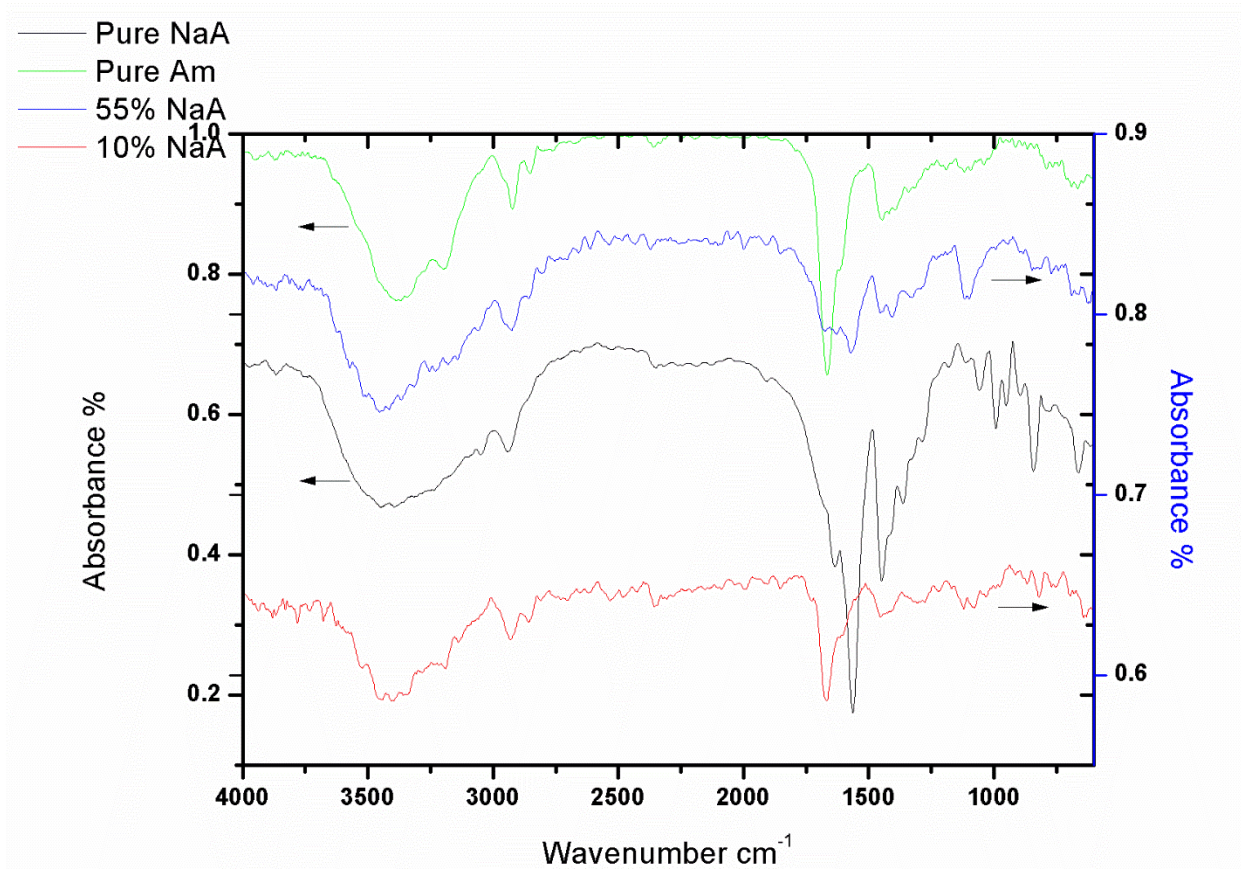


Figure 5- 3 rescaled spectrum of 10% and 55% NaA.

Since the absorbance of 10% and 55% NaA is too small compared to the absorbance of homopolymer, the 10% and 55% NaA spectrum was rescaled and magnified, as shown in Figure 5- 3. The arrow indicates the corresponding absorbance axis.

The base line of two peaks is set by connecting a line within chosen range. The method is depicted in Figure 5- 4, and Figure 5- 5 below. The peak area is calculated by OriginPro®. The relative absorbance is calculated according to the following equation:

$$A_{rel} = \frac{A_{1410}}{A_{2950}} \quad (5-1)$$

where A_{rel} is the relative absorbance and A_{1410} and A_{2950} represent the peak area under 1410 cm^{-1} and 2950 cm^{-1} , respectively.



Figure 5- 4 Chosen band and method of calculation of relative peak area. The spectrum is 55% NaA monomer concentration.

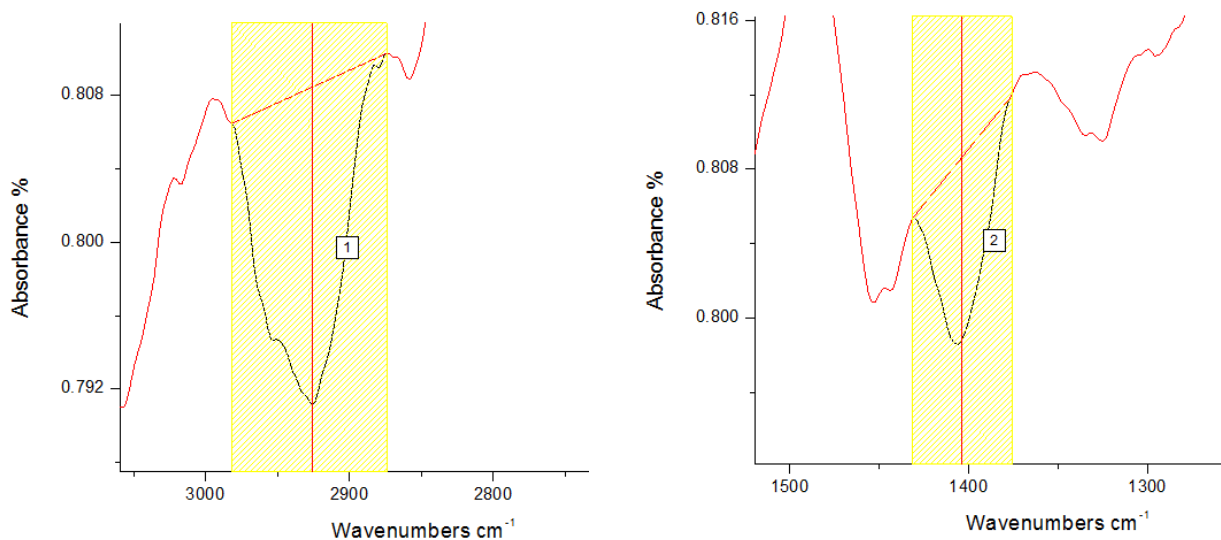


Figure 5- 5 (left) Magnified image for Figure 5- 4 at 1st peak area around 2950 cm⁻¹. (right) Magnified image for Figure 5- 4 at 2nd peak area around 1410 cm⁻¹

The acrylate content has a good linear correlation with the relative peak area, which is shown in Figure 5- 6. The relation is obtained by a linear-regression method, as follows:

$$NaA\% = -8.6675 + 194.6867A_{rel} \quad (5-2)$$

The increase in calculated relative absorbance is matched with the increase in acrylate content. At zero acrylate content (polyacrylamide homopolymer), the relative absorbance is 0.5124, which corresponds to weak amine stretch of acrylamide. The y-axis intercepts at -8.6675 , which is similar to the value Magalhaes et al. reported: -8.83^{54} . The reported slope is smaller than it is in this study, which could be due to the cross-linker concentration difference.

Therefore, two levels of cross-linker concentration were studied, which are 0.1 and 0.2 grams of BIS in the monomer solution. The cross-linker effect is demonstrated in Figure 5- 7. The lower cross-linker concentration shows a higher A_{rel} value. The increasing cross-linker concentration

reduces the calculated relative absorbance. The same effect is shown in both 10% and 55% acrylate content.

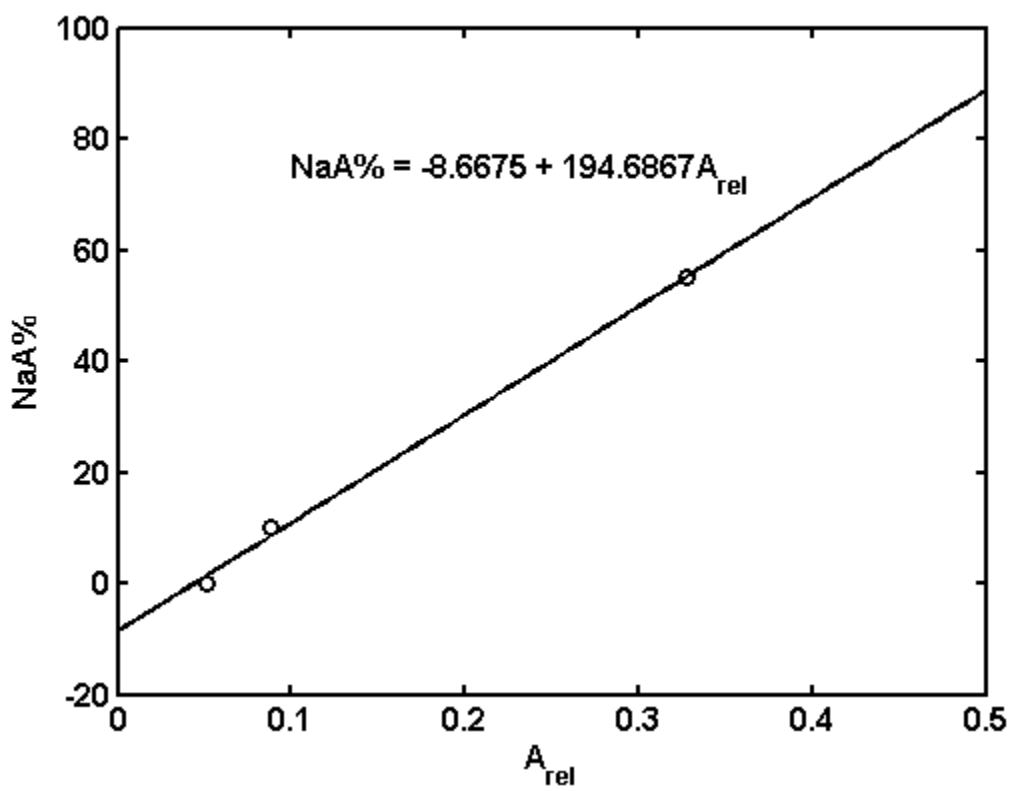


Figure 5-6 Acrylate content (F1) and relative peak area (Arel) relation for different copolymer composition.

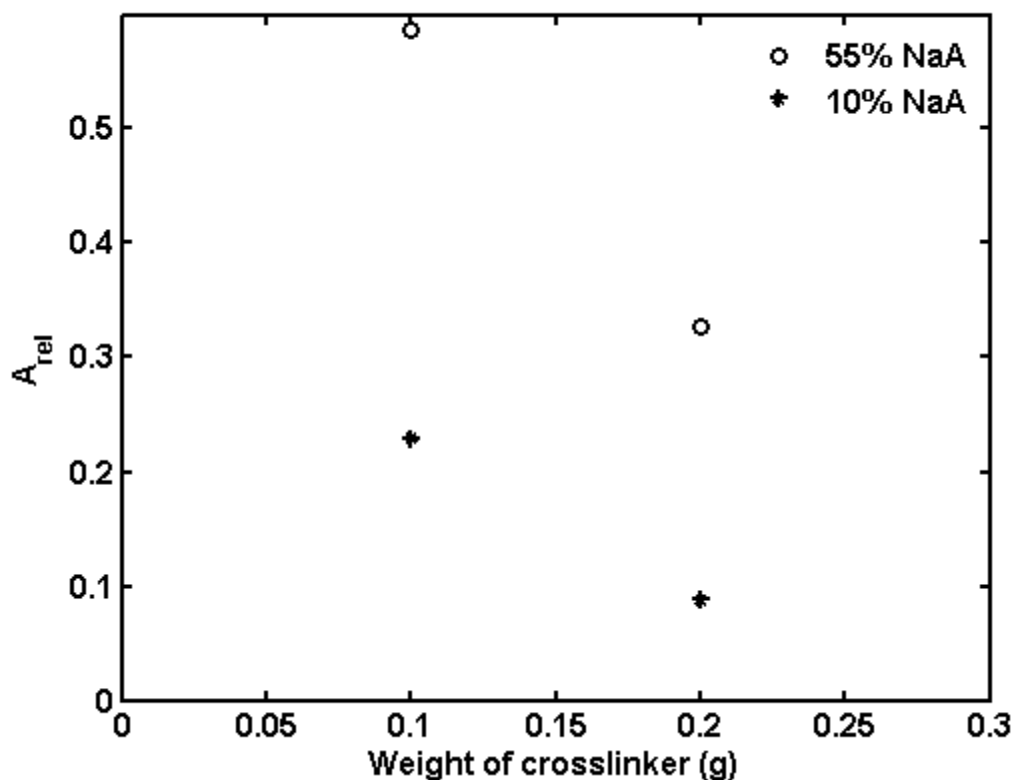


Figure 5- 7 Cross-linker effect on relative peak area.

5.3 Swelling test analysis and discussion:

Two important parameters of hydrogels are the equilibrium volume-swelling ratio (Q) and the number average molecular weight between crosslinks (\bar{M}_c)⁵⁵. The equilibrium volume-swelling ratio is the reciprocal of the polymer-volume fraction in the swollen state, which can be measured by the swelling test. The number average molecular weight between crosslinks determines the crosslinking density and porosity in hydrogel. Combining the equilibrium swelling theory and Flory-Huggins mixing theory, the \bar{M}_c can be calculated from swelling measurement with a few other important variables, such as the solvent-interaction parameter (χ_1).

Equilibrium Swelling Theory:

The polymer network will absorb solvent until the chemical potential of solvent in a free solution equals the chemical potential in the polymer network. Four terms contribute to the swelling equilibrium theory: the mixing of polymer with solvent (Π_{mix}), the elastic response due to crosslinking (Π_{elas}), the ionic contribution from the chemical potential inside and outside of polymer (Π_{ion}), and the electrostatic interaction of charges on the polymer chain (Π_{ele}). The equation can be written as follows⁵⁵:

$$\Pi_{mix} + \Pi_{elas} + \Pi_{ion} + \Pi_{ele} = 0 \quad (5-3)$$

For a non-ionic polymer, Π_{ion} and Π_{ele} are negligible. However, the acrylamide and sodium acrylate copolymer is an anionic polymer and those two terms cannot be negligible. However, according to the theoretical calculation and the experimental result, the Π_{ele} is typically small compared to the Π_{ion} . Therefore, the equilibrium equation simplifies to this:

$$\Pi_{mix} + \Pi_{elas} + \Pi_{ion} = 0 \quad (5-4)$$

The Π_{mix} contribution to the chemical potential can be derived from Flory-Huggins theory via the entropy change on the mixing, ΔS_{mix} , and the heat of mixing, ΔH_{mix} , as shown in Equation (5-5):

$$\Delta G_{mix} = \Delta H_{mix} - T\Delta S_{mix} \quad (5-5)$$

where T is the absolute temperature. The ΔH_{mix} is defined by liquid lattice theory as follows:

$$\Delta H_{mix} = z\Delta w_{12}x_1n_1v_{2,s} \quad (5-6)$$

To abbreviate the heat of mixing of two components, the Flory interaction parameter is introduced as follows:

$$\chi_1 = \frac{z\Delta w_{12}x_1}{KT} \quad (5-7)$$

where z is the lattice coordination number, Δw_{12} is the interchange energy due to unlike pair contacts, and x_1 is the number of segments in the solvent molecule⁵⁵. Substituting equation (5-7) into equation (5-6) yields:

$$\Delta H_{mix} = RT\chi_1 n_1 v_{2,s} \quad (5-8)$$

The entropy of mixing can be written as follows:

$$\Delta S_{mix} = -k(n_1 \ln v_{1,s} + n_2 \ln v_{2,s}) \quad (5-9)$$

where $v_{1,s}$ is the volume fraction of solvent and $v_{2,s}$ is the volume fraction of polymer. n_1 is the number of solvent molecules in a solution, n_2 is the number of polymer molecules in a solution, and k is the Boltzmann constant⁵⁵. In a crosslinked polymer system, the number of assumed uncrosslinked polymer molecules (n_2) equals to zero. So the overall equation can be simplified as follows:

$$\Delta G_{mix} = \Delta H_{mix} - T\Delta S_{mix} = KT[n_1 \ln v_{1,s} + \chi_1 n_1 v_{2,s}] \quad (5-10)$$

Differentiation of the above equation with respect to n_1 can be written as equation (5-11):

$$\Pi_{mix} = \left[\frac{RT}{V_1} \right] [\ln(1 - v_{2,s}) + v_{2,s} + \chi_1 v_{2,s}^2] \quad (5-11)$$

where R is the gas constant and T is the absolute temperature. The term $v_{2,s}$ is the polymer volume fraction in swollen state, which can be measured experimentally. V_1 is the solvent molar volume. In this case, water is used as a solvent, so V_1 is 18 cm³/mol. The χ_1 is the polymer-solvent interaction parameter according to the Flory-Huggins theory, which accounts for the free-energy change due to the mixing process. This variable is usually between 0 and 1; a higher value indicates a poor solvent for the polymer. χ_1 can be estimated by different approaches; however, they are not

usually applicable for strong hydrogel bonding. For this project, the χ_1 value is assumed to be equal to 0.48 for polyacrylamide and water interaction, according to Peppas et al.⁵⁵.

The elasticity term, Π_{elas} , accounts for the elastic response due to the crosslinking that is controlled by the effective crosslinking density (ρ_x). Increasing the crosslinking density decreases the water absorbance capacity since it reduces the number of possible configurations of the polymer chain and the movement of the polymer chain is limited. The general equation can be written as follows:

$$\Pi_{elas} = -RT\rho_x V_{2,r} \left[\left(\frac{V_{2,s}}{V_{2,r}} \right)^{\frac{1}{3}} - 0.5 \left(\frac{V_{2,s}}{V_{2,r}} \right) \right] \quad (5-12)$$

where $V_{2,r}$ is the polymer volume fraction in the solvent at a relaxed state: i.e., the volume fraction right after crosslinking but before swelling. For the polymer crosslinked in absence of solvent—i.e., for the crosslinking network prepared in bulk state— $V_{2,r}$ can be assumed to be 1. Therefore, the equation reduces to this:

$$\Pi_{elas} = -RT\rho_x \left[(v_{2,s})^{\frac{1}{3}} - 0.5(v_{2,s}) \right] \quad (5-13)$$

To extend the definition of crosslinking density, ρ_x is correlated with the number average molecular weight between crosslinks, \bar{M}_c , and the number average molecular weight of the polymer before crosslinking, \bar{M}_n . The relationship can be shown as follows:

$$\rho_x = \left[\frac{1}{v\bar{M}_c} \right] \left[1 - \frac{2\bar{M}_c}{\bar{M}_n} \right] \quad (5-14)$$

The number average molecular weight before crosslinking can be measured by using conventional Gel Permeation Chromatography methods. If crosslinking density is obtained by back calculation through swelling measurement, and if \bar{M}_n is obtained by GPC, the number average molecular

weight between crosslink can be easily calculated. The decreasing of ρ_x indicates a larger average

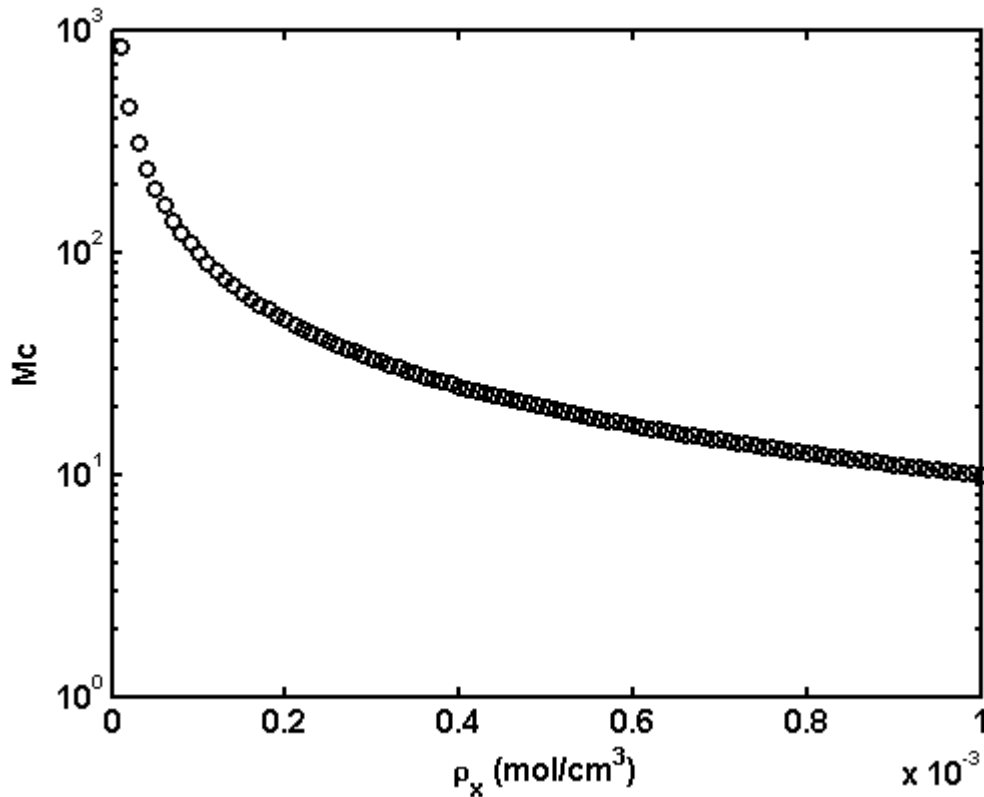


Figure 5- 8 crosslinking density ρ_x and number average molecular weight between crosslinking (\bar{M}_c) plot.

molecular weight between crosslinks, so the polymer chain is less crosslinked. Figure 5- 8 illustrates the relationship between crosslinking density and number average molecular weight between crosslinking, assuming number average molecular weight before crosslinking is 10000 and $v = 100 \text{ cm}^3/\text{mol}$. With an increase in the crosslinking density (from 10^5 to 10^3 mol/cm^3), the \bar{M}_c decreases from 833 to ~ 10 . A smaller \bar{M}_c value means that there are fewer chains between crosslinks; therefore, the polymer is more crosslinked. The value of \bar{M}_n is usually much greater than the value of \bar{M}_c , and the equation 5-14 can be simplified to with the assumption of $\bar{M}_c \gg \bar{M}_n$, as follows:

$$\rho_x = \left[\frac{1}{vM_c} \right]. \quad (5-15)$$

This assumption is valid if \bar{M}_n is very high; usually \bar{M}_n is on the order of 10^4 or higher. This can be verified by plotting crosslinking density versus \bar{M}_c at different \bar{M}_n values, as in Figure 5- 9. It clearly shows that the tendency of the curve is not affected by a change in \bar{M}_n when \bar{M}_n is greater than 10^4 .

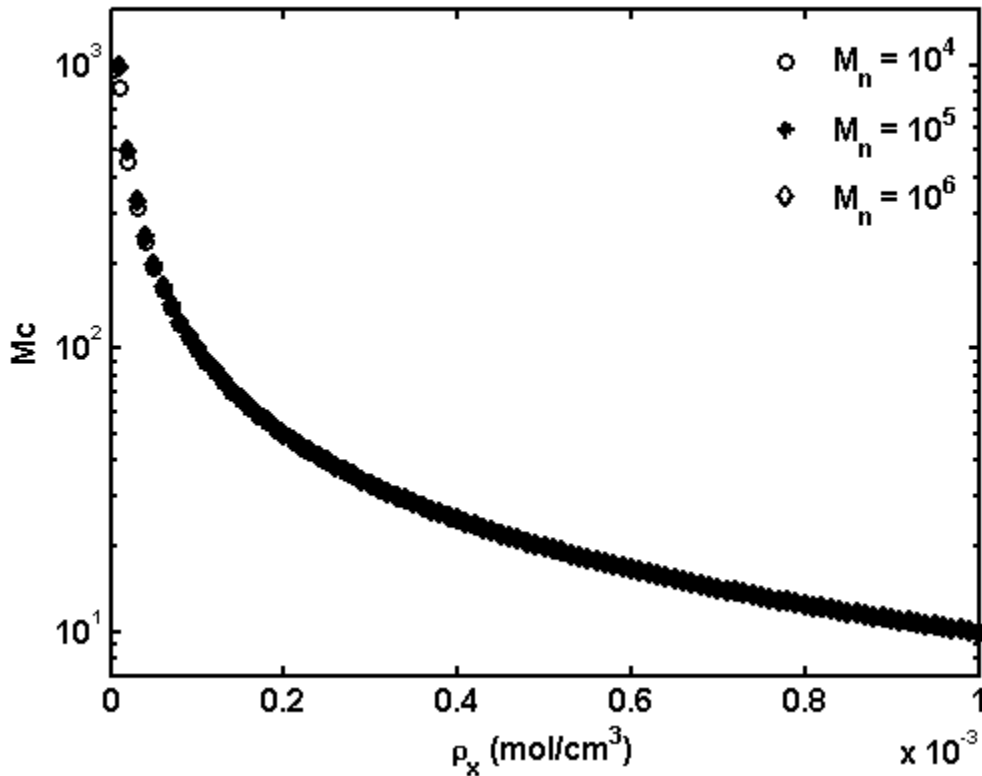


Figure 5- 9 Crosslinking density vs. \bar{M}_c at different \bar{M}_n value.

Since poly(acrylamide-co-sodium acrylate) is an anionic polymer, the Π_{ion} term that accounts for the osmotic swelling pressure due to the ion concentration difference cannot be ignored. The ionisable group in polymers must be maintained electro-neutral against the counter-ions that arise from the dissociation. Therefore, this term is significant in the ionic polymer network. The equation is given by,

$$\Pi_{ion} = RT \left[\frac{i v_{2,s}}{V_m} + v(c'_s - c_s) \right] \quad (5-16)$$

where i is the fraction of ionized polymer structural units in polymer chain, V_m is the molar volume of the monomer unit, v is the number of ions in solvent, c'_s and c_s are the concentrations of salt within the gel and in solution that came from external solvent, respectively. In this study, pure DI water with a pH of 7 is used as a solvent for the swelling test. Therefore, the second term in the equation (5-16) can be assumed to be zero. The equation simplifies to the following:

$$\Pi_{ion} = RT \left[\frac{i v_{2,s}}{V_m} \right] \quad (5-17)$$

Combining all these three equations leads to equation (5-18):

$$\frac{[\ln(1 - v_{2,s}) + v_{2,s} + \chi_1 v_{2,s}^2]}{V_1} + \rho_x \left[(v_{2,s})^{\frac{1}{3}} - 0.5(v_{2,s}) \right] + \frac{i v_{2,s}}{V_m} = 0 \quad (5-18)$$

The volume degree of swelling (Q), which equals the inverse of $v_{2,s}$, can be represented and calculated as a function of χ_1 , ρ_x , i , V_1 and V_m .

According to Flory-Huggins theory, a decrease in crosslinking density and the increasing of ionic content in the polymer network improves the swelling ratio of hydrogel. The swelling ratio is proportional to the ionic content in hydrogel and is inversely proportional to the crosslinking density, as shown in Figure 5- 10.

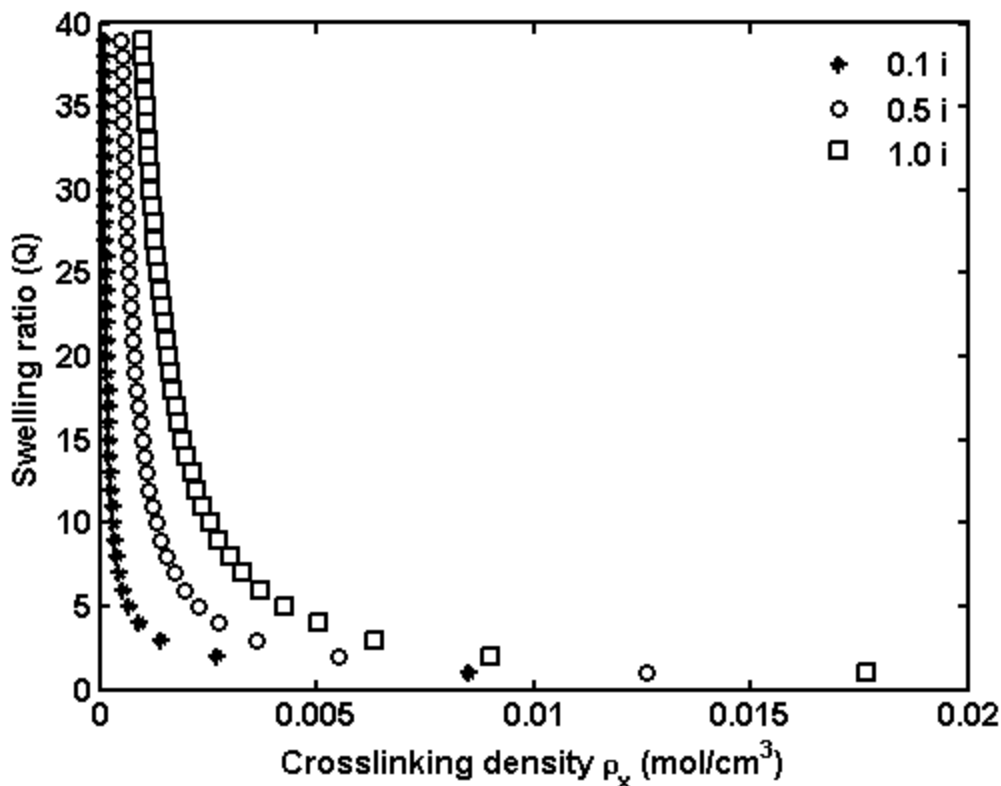


Figure 5- 10 Theoretical swelling curves for ionic polymer network. Assuming $V_{2,r} = 1$.

Assuming that the polymer chains are Gaussian chains, $V_m = 90 \text{ cm}^3/\text{mol}$, $V_1 = 10 \text{ cm}^3/\text{mol}$ for water molar volume, $\chi_1 = 0.48$ ⁵⁵. When the ionic content is increased at constant crosslinking density, the swelling ratio is (Q) increased. When crosslinking density is increased at constant ionic content, the swelling ratio decreases, so the water absorbance capacity decreases.

Experimental result analysis:

The dried polymer micro-particles with different monomer composition is placed into the cell-culture well plate, and the original size is recorded using a microscope. When DI water is added, the micro-particle swell quickly and the swelling process is recorded by microscope, as shown in Figure 5- 11. The volume increases 4 to 36 times for different monomer compositions and different crosslinker concentrations.

Micro-particle diameter was measured by ImageJ® three times, and the average value with error bar was plotted in Figure 5- 12. The micro-particles expand exponentially in the first 20 seconds,

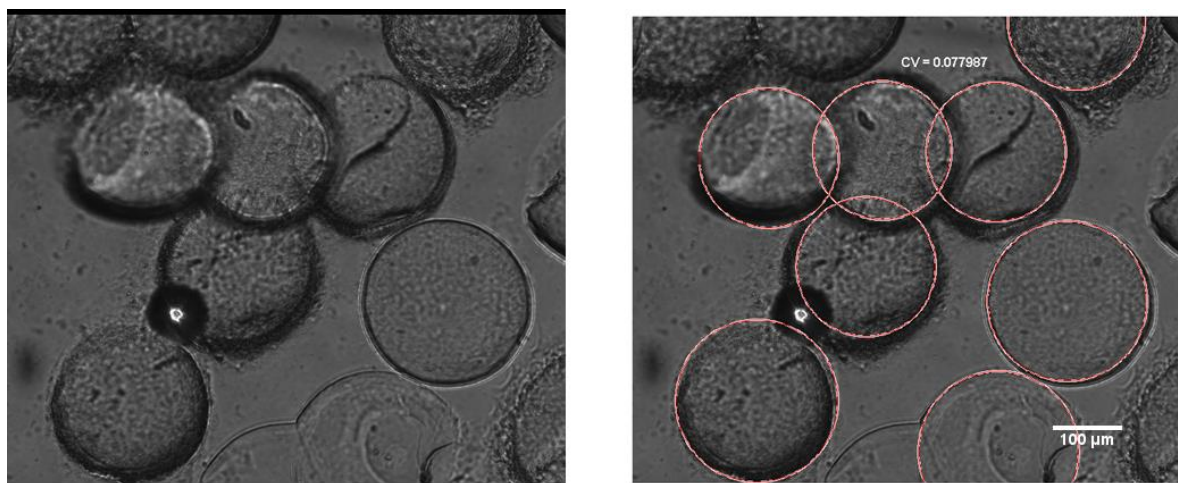


Figure 5- 11 Hydrogel micro-particles after swelling (right) Matlab program processed image (left).

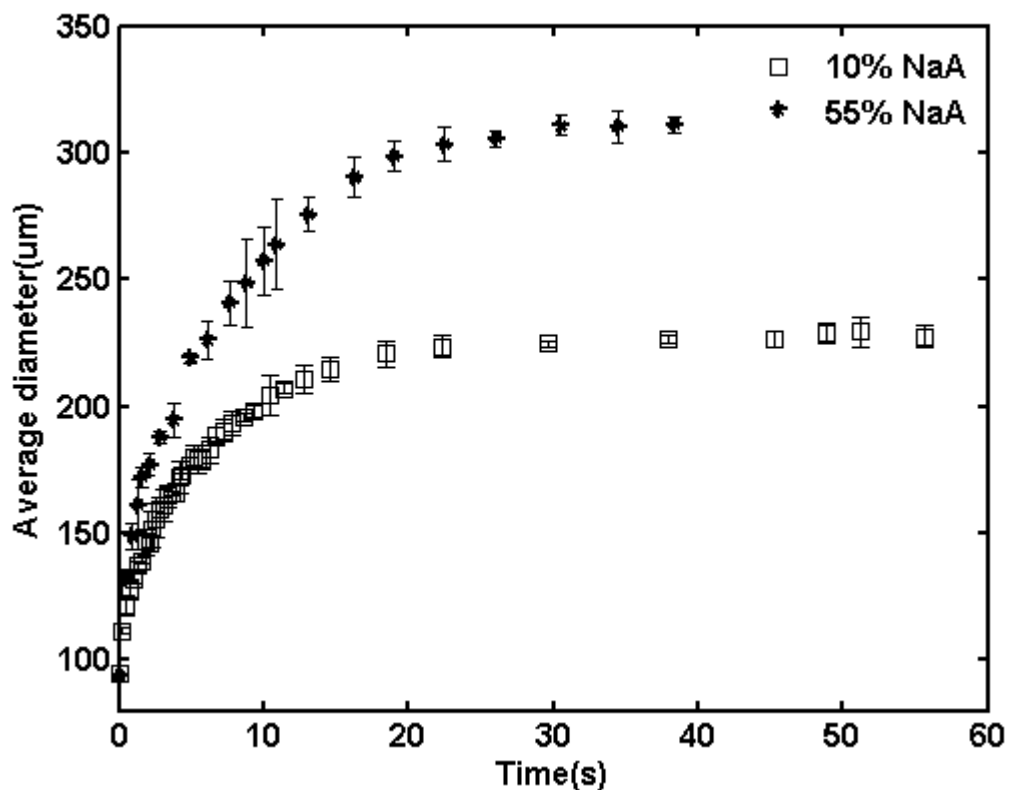


Figure 5- 12 Hydrogel micro-particles swelling experimental result average diameter vs. swelling time. The crosslinker concentration fixed at 0.2 w/v%.

and the volume after swelling reaches an equilibrium after 30 seconds. The volume does not

change much if additional water is added. According to Figure 5- 13, the initial size of micro-particle is similar for 10% and 55% NaA content in the feeding composition. After swelling, the diameter of 10% NaA micro-particles is only 2/3 that of 55% NaA micro-particle. The polymer fraction in the swollen state can be calculated from diameter change using equation 5-19:

$$Q = \frac{V}{V_0} = \frac{\frac{4}{3} \times \pi \times \left(\frac{D}{2}\right)^3}{\frac{4}{3} \times \pi \times \left(\frac{D_0}{2}\right)^3} = \left(\frac{D}{D_0}\right)^3 \quad (5-19)$$

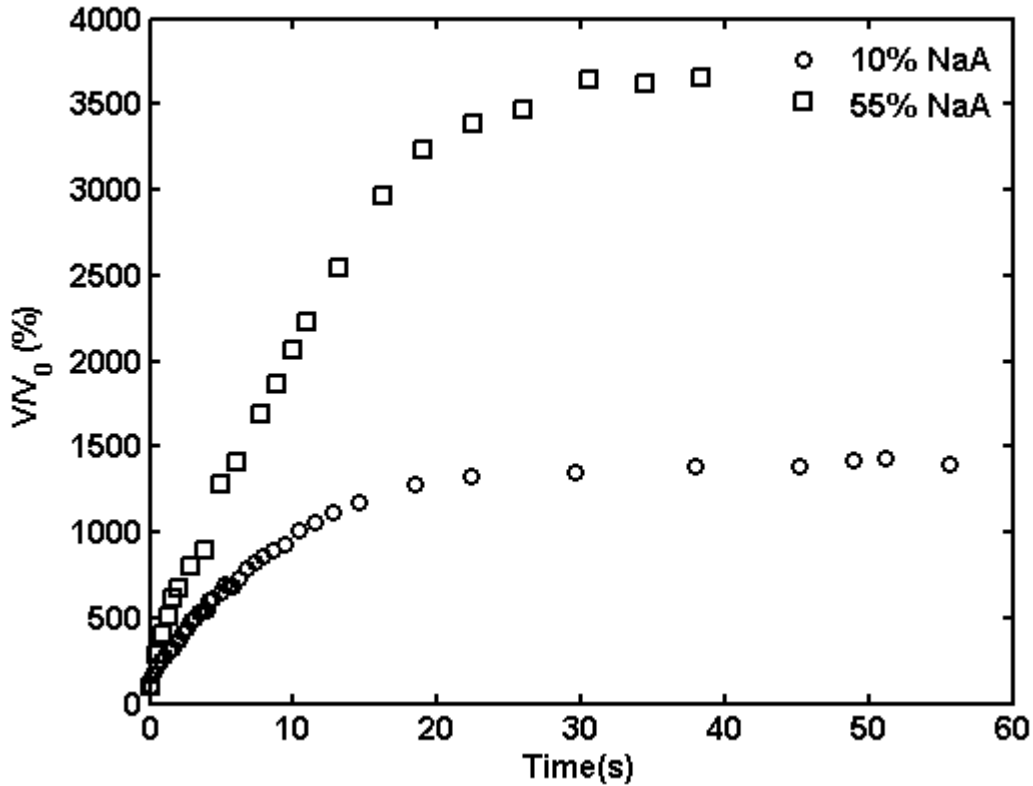


Figure 5- 13 Hydrogel micro-particles swelling experimental result average swelling ratio vs. swelling time. The crosslinker concentration fixed at 0.2 w/v%.

After swelling, the dried micro-particle expands to almost 40 times its original size for 55% NaA copolymer. The 10% NaA copolymer has a smaller swelling ratio (~14 times). The larger swelling ratio is contributed to the higher ionic content in 55% NaA copolymer, which is in agreement with the Flory-Huggins theory.

The effect of crosslinker concentration is studied in this project. 0.1 and 0.2 grams of crosslinker was used for different monomer compositions. The crosslinker concentration is inversely proportional to the swelling ratio, as shown in Figure 5- 14, which is in agreement with the Flory-Huggins theory. The higher crosslinker concentration results in higher crosslinking density and in a smaller number of average molecular weight between crosslinks; therefore, the swelling is less.

Compared to the bulk hydrogel, the micro-particles not only swell faster but the swelling ratio is also higher, especially when the ionic content is at a high level. From Figure 5- 15, the swelling ratio is same for the polyacrylamide homopolymer obtained from bulk and microfluidic chip. At 10% of sodium acrylate content, the swelling ratio of micro-particles is 47.12% higher than that of bulk. At 55% of sodium acrylate content, the swelling ratio of micro-particles is 126.49% higher than that of bulk.

The micro-particle has a large surface-to-volume ratio compared to that of bulk; therefore, micro-particle swelling is much faster than in bulk. During polymerization, the oil phase instantaneously removes the heat released from droplet polymerization. Therefore, the micro-particles have a more uniform crosslink in the surface and core compared to the bulk. So the water can penetrate to the core of micro-polymer faster than in bulk.

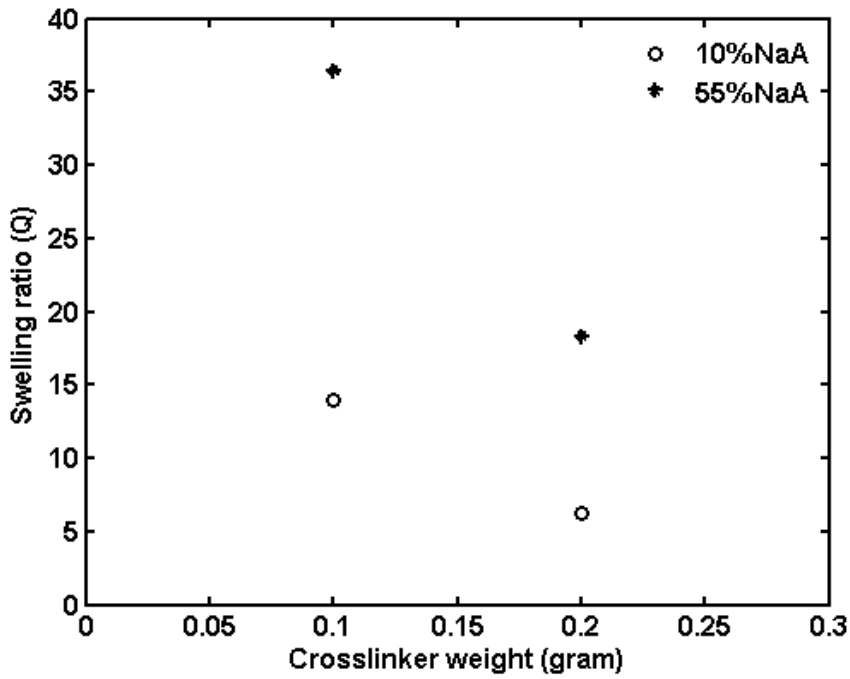


Figure 5- 14 The effect of crosslinker concentration on swelling ratio.

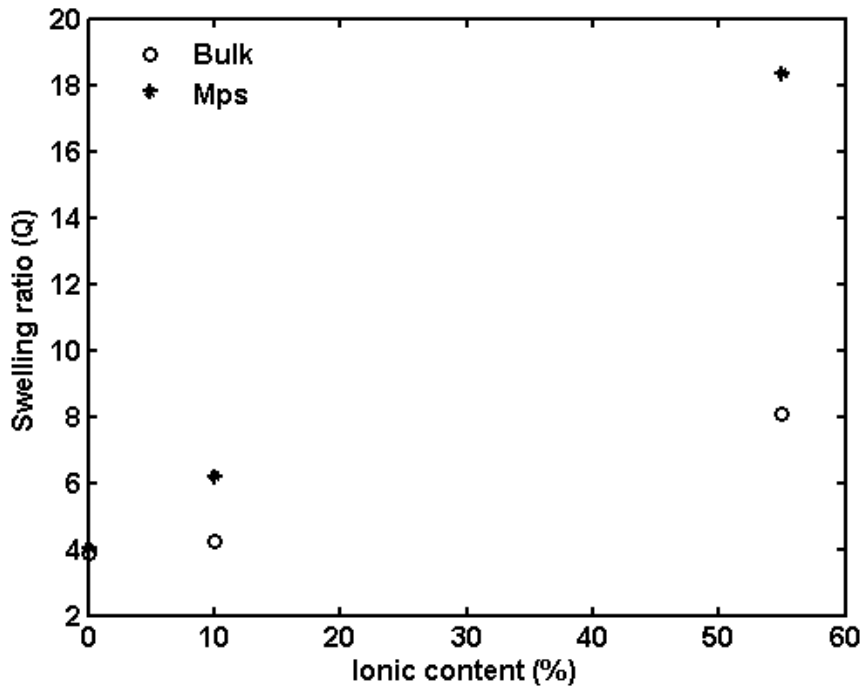


Figure 5- 15 The effect of ionic content% on swelling ratio.

According to equation (5-18), the measured swelling ratio is related to the crosslinking density (ρ_x) and the ionic content (i). For the polyacrylamide homopolymer, the ionic content is zero, so we estimate the ρ_x , which equals 8.33×10^{-4} . We can assume that the crosslinking density is independent of the feed composition if the crosslinker concentration and the total monomer concentration are fixed. Therefore, the same value of ρ_x is applied to the other polymer system if the crosslinker concentration and the total monomer concentration are the same. The theoretical ionic content can be calculated based on equation (5-18), as shown in Figure 5- 16. The theoretical ionic content is smaller than the experimental result. This can be explained by the fact that the effective ionic content is smaller than the feed ionic composition. The deviation is small at lower feed ionic content but increases dramatically at the high-feed ionic composition. A similar phenomena is reported by Okay et al.⁵⁶

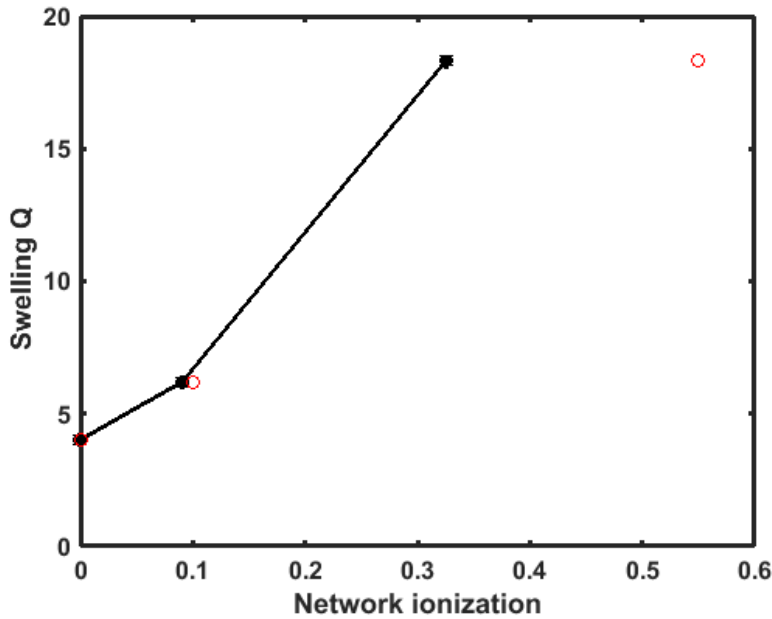


Figure 5- 16 The experimental result and theoretical value comparison. Red circle is the experimental measurement. Black dot is the calculated theoretical value.

Chapter 6: Summary, Conclusion and Future Work

In this work, an experiment method is developed to synthesize poly (acrylamide-co-sodium acrylate) hydrogel micro-particles in microfluidic devices. On-chip and off-chip methods are evaluated. The inverted-chip method produces monodispersed spherical hydrogel micro-particles. The properties of micro-particles (with various monomer composition and crosslinker concentration) were analyzed, such as volume swelling ratio, composition, size and size distribution. The swelling property was controlled by the ionic content and crosslinker concentration. The swelling ratio obtained from the swelling test matches the Flory-Huggins theory and the equilibrium swelling theory.

Future work and recommendations:

- In this work, only two levels of NaA feed composition are synthesized and tested. For deep understanding of swelling mechanism, more experiment with different feed compositions are required.
- In this study, DEAP is used as photo-initiator. It has higher solubility in oil than in water. Therefore, adding DEAP is necessary to maintain the initiator concentration in monomer. If the initiator switches to a water-soluble initiator, this problem will be avoided, which can save oil and initiator in reservoir.
- The conversion is generally measured by gravimetry in conventional polymer synthesis. However, the gravimetry is difficult to perform in this work, since the amount of product is too low. It may be useful to do additional characterization to understand conversion in MF.

- The reaction time is limited by the cylinder height and intensity of the UV lamp. Therefore, a longer cylinder or stronger UV intensity may increase the conversion so that MPs can be synthesised at a lower total monomer and initiator concentration.
- MPs production can be scaled using multiple MFs or multiple micro-channels in a MF.

Reference:

1. Capretto, L. *et al.* Production of polymeric micelles by microfluidic technology for combined drug delivery : Application to osteogenic differentiation of human periodontal ligament mesenchymal stem cells (hPDLSCs). *Int. J. Pharm.* **440**, 195–206 (2013).
2. Vladislavljevi, G. T. *et al.* Industrial lab-on-a-chip : Design , applications and scale-up for drug discovery and delivery ☆. **65**, 1626–1663 (2013).
3. Zhao, C., He, L., Zhang, S. & Middelberg, A. P. J. Nanoparticle synthesis in microreactors. *Chem. Eng. Sci.* **66**, 1463–1479 (2011).
4. Çavuş, S., Gürdag, G., Sözgen, K. & Gürkaynak, M. A. The preparation and characterization of poly(acrylic acid-co-methacrylamide) gel and its use in the non-competitive heavy metal removal. *Polym. Adv. Technol.* **20**, 165–172 (2009).
5. Yeh, C.-H., Lin, P.-W. & Lin, Y.-C. Chitosan microfiber fabrication using a microfluidic chip and its application to cell cultures. *Microfluid. Nanofluidics* **8**, 115–121 (2010).
6. Lin, M., Zhang, G., Hua, Z., Zhao, Q. & Sun, F. Colloids and Surfaces A : Physicochemical and Engineering Aspects Conformation and plugging properties of crosslinked polymer microspheres for profile control. *Colloids Surfaces A Physicochem. Eng. Asp.* **477**, 49–54 (2015).
7. Ahmed, E. M. Hydrogel : Preparation , characterization , and applications : A review. *J. Adv. Res.* **6**, 105–121 (2015).
8. Rousseau, D. & Chauveteau, G. Rheology and transport in porous media of new water shutoff/conformance control microgels. ... *Symp. Oilf.* ... (2005). at <<http://www.onepetro.org/mslib/servlet/onepetroreview?id=00093254>>
9. Abdalbaki, M., Huh, C., Sepehrnoori, K., Delshad, M. & Varavei, A. A critical review on use of polymer microgels for conformance control purposes. *J. Pet. Sci. Eng.* **122**, 741–753 (2014).
10. Al-maamari, R., Al-shabibi, I., Mansoor, A., Al-sharji, H. & Zaitoun, A. Mechanical Stability of High-Molecular-Weight Polyacrylamides and an (acrylamido tert -butyl sulfonic acid)– Acrylamide Copolymer Used in Enhanced Oil Recovery. **40921**, 6–11 (2014).
11. Dupuis, G. & Al-Maamari, A. Mechanical and Thermal Stability of Polyacrylamide-based Microgel Products for EOR. *SPE Int. Symp. Oilf. Chem. Symp. Oilf.* 1–11 (2013). at <<http://www.onepetro.org/mslib/servlet/onepetroreview?id=SPE-164135-MS>>
12. Qiu, Y., Wei, M., Geng, J. & Wu, F. Successful Field Application of Microgel Treatment in High Temperature High Salinity Reservoir in China. **2002**, (2016).
13. Yao, C. *et al.* Enhanced Oil Recovery Using Micron-Size Polyacrylamide Elastic Microspheres : Underlying Mechanisms and Displacement Experiments. *Ind. Eng. Chem. Res.* 10925–10934 (2015). doi:10.1021/acs.iecr.5b02717
14. Iwasaki, T. & Yoshida, J. Free Radical Polymerization in Microreactors. Significant Improvement in Molecular Weight Distribution Control. *Macromolecules* **38**, 1159–1163 (2005).

15. Shepherd, R. F. *et al.* Microfluidic assembly of homogeneous and janus colloid-filled hydrogel granules. *Langmuir* **22**, 8618–8622 (2006).
16. Choi, C.-H., Jung, J.-H., Kim, D.-W., Chung, Y.-M. & Lee, C.-S. Novel one-pot route to monodisperse thermosensitive hollow microcapsules in a microfluidic system. *Lab Chip* **8**, 1544 (2008).
17. Ikkai, F., Iwamoto, S., Adachi, E. & Nakajima, M. New method of producing mono-sized polymer gel particles using microchannel emulsification and UV irradiation. *Colloid Polym. Sci.* **283**, 1149–1153 (2005).
18. Wei, J. *et al.* Multi-Stimuli-Responsive Microcapsules for Adjustable Controlled-Release. *Adv. Funct. Mater.* n/a–n/a (2014). doi:10.1002/adfm.201303844
19. Sugiura, S., Nakajima, M., Itou, H. & Seki, M. Synthesis of polymeric microspheres with narrow size distributions employing microchannel emulsification. *Macromol. Rapid Commun.* **22**, 773–778 (2001).
20. Serra, C. a. & Chang, Z. Microfluidic-assisted synthesis of polymer particles. *Chem. Eng. Technol.* **31**, 1099–1115 (2008).
21. Kumacheva, E. *Microfluidic Reactors for Polymer Particles.* (2011).
22. Wu, T., Mei, Y., Cabral, J. T., Xu, C. & Beers, K. L. A new synthetic method for controlled polymerization using a microfluidic system. *J. Am. Chem. Soc.* **126**, 9880–9881 (2004).
23. Voicu, D. *et al.* Kinetics of multicomponent polymerization reaction studied in a microfluidic format. *Macromolecules* **45**, 4469–4475 (2012).
24. Honda, T., Miyazaki, M., Nakamura, H. & Maeda, H. Controllable polymerization of N-carboxy anhydrides in a microreaction system. *Lab Chip* **5**, 812–818 (2005).
25. Kundu, S. *et al.* Continuous Flow Enzyme-Catalyzed Polymerization in a Microreactor. *J. Am. Chem. Soc.* **133**, 6006–6011 (2011).
26. Fukuyama, T., Kajihara, Y., Ryu, I. & Studer, A. Nitroxide-mediated polymerization of styrene, butyl acrylate, or methyl methacrylate by microflow reactor technology. *Synth.* **44**, 2555–2559 (2012).
27. Kawakatsu, T., Kikuchi, Y. & Nakajima, M. Regular-sized cell creation in microchannel emulsification by visual microprocessing method. *J. Am. Oil Chem. Soc.* **74**, 317–321 (1997).
28. Sugiura, S., Nakajima, M., Iwamoto, S. & Seki, M. interfacial tension Driven monodispersed droplet Formation from Microfabricated Channel Array. *Langmuir* 5562–5566 (2001).
29. Liu, X.-S. *et al.* Preparation of Monodisperse Poly(pentaerythritol triacrylate) Microspheres using a T-junction Microfluidic Chip. *Integr. Ferroelectr.* **146**, 43–47 (2013).
30. Nisisako, T., Torii, T. & Higuchi, T. Novel microreactors for functional polymer beads. *Chem. Eng. J.* **101**, 23–29 (2004).
31. Choi, C. H. *et al.* Generation of monodisperse alginate microbeads and in situ encapsulation of cell in microfluidic device. *Biomed. Microdevices* **9**, 855–862 (2007).
32. Anna, S. L., Bontoux, N. & Stone, H. a. Formation of dispersions using ‘flow focusing’ in microchannels. *Appl. Phys. Lett.* **82**, 364–366 (2003).

33. Li, W. *et al.* Multi-step microfluidic polymerization reactions conducted in droplets: The internal trigger approach. *J. Am. Chem. Soc.* **130**, 9935–9941 (2008).
34. Abate, A. R. *et al.* Synthesis of monodisperse microparticles from non-newtonian polymer solutions with microfluidic devices. *Adv. Mater.* **23**, 1757–1760 (2011).
35. Lewis, P. C. *et al.* Continuous Synthesis of Copolymer Particles in Microfluidic Reactors. *Macromolecules* **38**, 4536–4538 (2005).
36. Dang, T. D., Kim, Y. H., Kim, H. G. & Kim, G. M. Preparation of monodisperse PEG hydrogel microparticles using a microfluidic flow-focusing device. *J. Ind. Eng. Chem.* **18**, 1308–1313 (2012).
37. Yang, C. H., Huang, K. S., Lin, P. W. & Lin, Y. C. Using a cross-flow microfluidic chip and external crosslinking reaction for monodisperse TPP-chitosan microparticles. *Sensors Actuators, B Chem.* **124**, 510–516 (2007).
38. Seiffert, S., Friess, F., Lendlein, A. & Wischke, C. Faster droplet production by delayed surfactant-addition in two-phase microfluidics to form thermo-sensitive microgels. *J. Colloid Interface Sci.* **452**, 38–42 (2015).
39. Yang, B., Lu, Y. & Luo, G. Controllable preparation of polyacrylamide hydrogel microspheres in a coaxial microfluidic device. *Ind. Eng. Chem. Res.* **51**, 9016–9022 (2012).
40. Jeong, W. J. *et al.* Continuous fabrication of biocatalyst immobilized microparticles using photopolymerization and immiscible liquids in microfluidic systems. *Langmuir* **21**, 3738–3741 (2005).
41. Chang, Z. *et al.* Multiscale materials from microcontinuous-flow synthesis: ZnO and Au nanoparticle-filled uniform and homogeneous polymer microbeads. *Nanotechnology* **21**, 015605 (2010).
42. Khan, I. U. *et al.* Microfluidic conceived drug loaded Janus particles in side-by-side capillaries device. *Int. J. Pharm.* **473**, 239–249 (2014).
43. Yang, Y.-T. *et al.* A side-by-side capillaries-based microfluidic system for synthesizing size- and morphology-controlled magnetic anisotropy janus beads. *Adv. Powder Technol.* **26**, 156–162 (2015).
44. Chang, Z., Serra, C. a, Bouquey, M., Prat, L. & Hadziioannou, G. Co-axial capillaries microfluidic device for synthesizing size- and morphology-controlled polymer core-polymer shell particles. *Lab Chip* **9**, 3007–3011 (2009).
45. Dendukuri, D., Pregibon, D. C., Collins, J., Hatton, T. A. & Doyle, P. S. Continuous-flow lithography for high-throughput microparticle synthesis. *Nat. Mater.* **5**, 365–369 (2006).
46. Dendukuri, D., Tsoi, K., Hatton, T. A. & Doyle, P. S. Controlled synthesis of nonspherical microparticles using microfluidics. *Langmuir* **21**, 2113–2116 (2005).
47. Yu, B. *et al.* Preparation of monodisperse PEG hydrogel composite microspheres via microfluidic chip with rounded channels. *J. Micromechanics Microengineering* **23**, 095016 (2013).
48. Gunduz, O., Ahmad, Z., Stride, E. & Edirisinghe, M. A device for the fabrication of multifunctional particles from microbubble suspensions. *Mater. Sci. Eng. C* **32**, 1005–1010 (2012).
49. Vasiliauskas, R. *et al.* Simple Microfluidic Approach to Fabricate Monodisperse Hollow Microparticles for Multidrug Delivery. *ACS Appl. Mater. Interfaces* 150702130220008 (2015). doi:10.1021/acsami.5b04824

50. Ono, T., Yamada, M., Suzuki, Y., Taniguchi, T. & Seki, M. One-step synthesis of spherical/nonspherical polymeric microparticles using non-equilibrium microfluidic droplets. *RSC Adv.* **4**, 13557 (2014).
51. Xia, Y. & Whitesides, G. M. Soft Lithography. *Angew. Chemie Int. Ed.* **37**, 550–575 (1998).
52. Whitesides, G. M., Michinao, H., Piotr, G. & Howard A., S. *Soft Matter.* **4**, (2008).
53. Seiffert, S., Dubbert, J. & Weitz, D. A. Lab on a Chip Reduced UV light scattering in PDMS microfluidic devices. 966–968 (2011). doi:10.1039/c0lc00594k
54. Magalhães, A. S. G. & Neto, M. P. A. *Quim. Nova.*, **35**, 1464–1467 (2012).
55. Brannon, L.-P. & Harland, R. S. *Absorbent Polymer Technology.* Elsevier (2008). doi:10.1016/S0167-5648(08)71009-8
56. Okay, O. & Sariisik, S. B. Swelling behavior of poly (acrylamide-co-sodium acrylate) hydrogels in aqueous salt solutions: theory versus experiments. *Eur. Polym. J.* **36**, 393–399 (2000).